FATE AND TRANSPORT OF POLYMERIC NANOPARTICLES IN SATURATED POROUS MEDIA

A Thesis

by

JONATHAN E. SANDERS

Submitted to the Office of Graduate and Professional Studies of
Texas A&M University
in partial fulfillment of the requirements for the degree of

MASTER OF SCIENCE

Chair of Committee,	Gretchen Miller
Committee Members,	Peter Knappett
	Karen Wooley
	Qi Ying
Head of Department,	Robin Autenrieth

August 2015

Major Subject: Civil Engineering

ABSTRACT

The application of engineered nanomaterials has improved many traditional groundwater remediation technologies; however, the development of novel nano-scale remediation technologies remains limited. magnetic shell crosslinked knedel-like (MSCKs) are novel polymeric nanoparticles whose application towards groundwater remediation is promising. MSCKs differ from traditional remediation technologies in that they are non-reactive and highly selective for specific contaminants.

MSCKs are spherical particles with a hydrophilic shell and hydrophobic core which entraps suspended iron oxide nanoparticles, rendering MSCKs magnetic. MSCKs operate like discrete surfactant packets: increasing the mobility and apparent solubility of hydrophobic species, but doing so within the confines of discrete particles which can then be recovered by filtration or magnetic removal. MSCKs accomplish this *via* the sequestration of hydrophobic species through the shell and into the core where the hydrophilic environment is able to entropically stabilize the contaminant. In aqueous phase benchtop tests, MSCKs have been shown to sequester ten times their mass of crude oil.

This study explores the transport characteristics and contaminant sequestration capabilities of MSCKs in saturated porous media. Transport characteristics were determined via one dimensional impulse column experiments in columns containing a saturated sand or a saturated sand/clay mixture. Sequestration experiments were determined under identical conditions, with aqueous phase contaminant sequestration being done in ambient 8.66 mg/L *m*-xylene $_{(aq)}$ and free phase contaminant sequestration

being conducted in a column with roughly 5% of the pore space occupied by free phase mineral oil.

The results of these column studies indicated that MSCKs readily transport through saturated sand with virtually no loss in recovery but that in the presence of clays, MSCK transport is retarded *via* irreversible attachment and/or aggregation and straining of MSCKs. The presence of hydrocarbons in either the aqueous phase or free phase also reduces the mobility of MSCKs and lowers recovery.

Additionally, this study has revealed that MSCKs can remove m-xylene $_{(aq)}$ to below the detection limit and well below the regulatory limits for residential groundwater. The sequestration of free phase mineral oil by MSCKs was significantly lower, with mineral oil recovery totaling between 3% and 10% of the total mass of MSCKs injected.

ACKNOWLEDGEMENTS

I would like to offer the following people my thanks and gratitude:

- my advisor, Dr. Gretchen Miller, for her patience, guidance, and encouragement, without which this project would never have been possible;
- my committee member Peter Knappett, for his knowledge of colloidal transport literature and willingness to offer opinions and advice;
- my committee member Dr. Karen Wooley for the use of her laboratory, instrumentation, and for her generous aid in funding this project;
- my fellow group members for their patience and advice in all the group meetings which I intentionally or inadvertently prolonged; and,
- all my family and friends, for bearing with me and being understanding throughout the course of this project.

I would like to also acknowledge the Texas Hazardous Waste Research Center (513TAM0031H) and the National Science Foundation (DMR-1105304) for partially funding this project

Finally, I would also like to give a special thanks to my wife, Adriana Pavia-Sanders who was a constant soundboard, reviewer, co-worker, inspiration, and motivator. Without her love, support, and effort, this project would never have been possible.

NOMENCLATURE

MSCK	Magnetic Shell Crosslinked Knedel-like Nanoparticles
USEPA	United States Environmental Protection Agency
BTC	Breakthrough Curve
CDF	Cumulative Distribution Function
CHP	Constant Head Permeameter

TABLE OF CONTENTS

LIST OF FIGURES

LIST OF TABLES

1. INTRODUCTION

1.1. Overview of Research

The objective of this research was to determine if magnetic shell crosslinked knedel-like (MSCKs) nanoparticles are a viable groundwater remediation technology. This project was intended to serve as a proof of concept study for future research into the use of MSCKs and MSCK derivatives in groundwater remediation. Although various other engineered nanoparticles (ENPs) have been studied for potential use as groundwater remediation tools, the application of polymeric amphiphilic ENPs for the remediation of groundwater has yet to be demonstrated [1, 2]. For the purposes of this research, the viability of MSCKs as a groundwater remediation technology was determined by the following criteria:

1) MSCKs readily transmit through saturated porous media;
2) MSCKs sequester aqueous phase contaminants during transport; and
3) MSCKs sequester non-aqueous phase contaminants during transport.

These criteria were assessed by conducting a column study using sand and sand clay mixtures in both the presence and absence of aqueous phase hydrocarbons and non-aqueous phase hydrocarbons.

1.2. Properties of Engineered Nanoparticles

Engineered nanomaterials (ENMs) are rigorously defined as materials which have at least one side measuring between 1 nanometer (10^{-9} m) and 0.1 micrometer (10^{-7} m) [3]. ENMs meeting these size constraints in one dimension are referred to as nano- or thin-films and are commonly applied as a surface coating to enhance the reactive, conductive,

or electrical properties of the parent material [4]. Discrete particles which meet the aforementioned size constraints in two or three dimensions are classified as ENPs and are much more mobile in the environment [5].

In general, ENPs typically fall into one of three broad categories, depending on their composition: polymeric/micelle, carbon-based, or metal/metal oxide. MSCKs fall into the polymeric/micelle category which, although increasingly popular in chemistry and materials science research, are uncommon in industrial or commercial settings and have yet to be fully explored in the environmental engineering literature. Carbon-based nanoparticles consist of Fullerenes (*e.g.,* C_{60} or, colloquially, Bucky Balls) and carbon nanotubes. Metal and metal oxide nanoparticles typically consist of a metal core with a solvent stabilized core (typically the oxidized metal) and are arguably the most researched ENP for environmental remediation applications [6, 7]. This focus is largely fueled by the size dependent toxicological properties of these ENPs, coupled with their widespread industrial use, and has led to considerable debate on how they should be classified, particularly when discussing ENPs as emerging contaminants [8, 9]. Nanoscale zero valent iron (nZVI) is of particular interest due to its widespread use in water treatment and groundwater remediation, particularly in permeable reactive barriers (PRBs).

When discussing ENMs, it is important to note the effect that particle size has on the properties of the material in question. Electrical, chemical, and physical interactions between ENMs and other materials typically occur at the surface of the ENM. Since volume and mass are linearly related, the surface area to volume ratio essentially

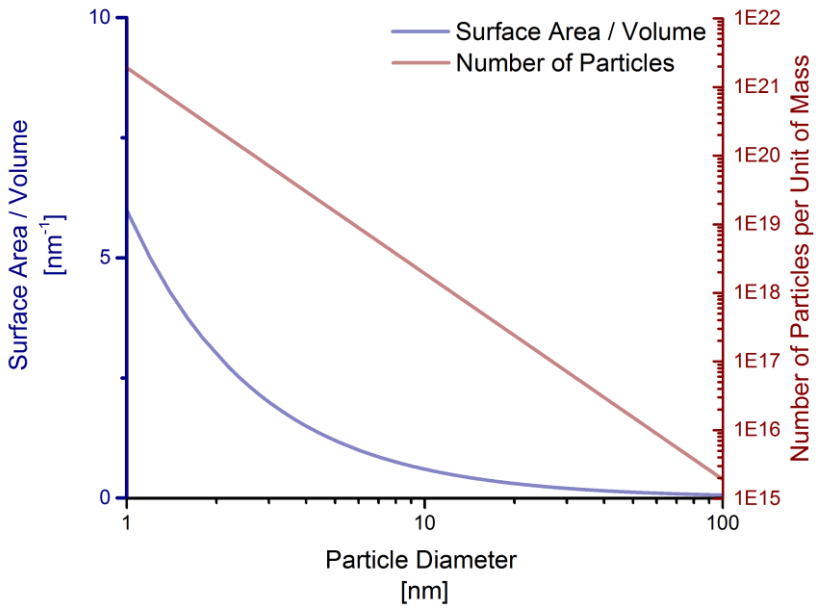

Figure 1 – Surface area to volume ratio as a function of particle diameter (blue line). Number of particles per unit mass as a function of particle diameter (red line). Assumes uniform spherical particles with a density of 1 g/cm^3.

describes the amount of surface area available to interact with external media per unit of mass of the ENM. For spherical ENPs, the surface area to mass ratio can be calculated by:

$$\frac{SA}{V * \rho} = \frac{\pi * d^2}{\frac{\rho}{6} * \pi * d^3} = \frac{6}{\rho * d}$$

where *SA* is the surface area, *V* is the volume, ρ is the density of the ENP, and *d* is the diameter of the spherical particle. As *d* decrease, the *SA/V* increases, meaning that the smaller the ENP, the more surface area is available per unit of mass. In addition to this increase in *SA/V*, smaller particle diameters mean that for a given mass of material, the number of particles also increases (Figure 1).

Another significant effect is that as particle size decreases, ENPs that are sufficiently small have also been observed to act as though they were a single atom or molecule with regard to electron and heat transfers and chemical reactions [8]. This molecular-like behavior is further emphasized when particle size is small enough that Brownian motion starts to outweigh gravitational effects. Because of these properties, suspended ENPs are able to disperse into dead spaces in porous media much more efficiently than larger particles while also enhancing the reaction kinetics for ENPs relative to bulk particles of the same composition [17]. The size and distribution of ENMs varies greatly depending composition and manufacturing process; however, most environmentally relevant ENPs are between 25 and 810 nm in diameter (*e.g.*, Table 1).

Table 1 - Common ENP size distribution

ENP type	Mean Particle Size (nm) (range given in parentheses)	Reference
C_{60}	75 (25-500)	10, 11
TiO_2	330 (175-810)	12
SiO_2	205 (135-510)	12
ZnO	480 (420-640)	12
Fe^0	>1000	13
Fullerol	100	14-16

1.3. Properties of MSCKs

MSCKs are spherical and monodisperse amphiphilic, polymeric nanoparticles which were first reported in 2013 [18]. MSCKs are assembled *via* the micellization of diblock copolymers of poly acrylic acid-*block*-poly styrene (PAA-*b*-PS) in the presence of oleic acid-stabilized iron oxide nanoparticles and are then crosslinked for stability. The resulting core-shell morphology (Figure 2), is flexible and permeable, allowing for the diffusion of hydrophobic pollutants into the hydrophobic core of the MSCK. This permits the entropic stabilization of hydrophobic species from the aqueous phase into the core of the MSCKs, essentially allowing MSCKs to act as discrete surfactant packets.

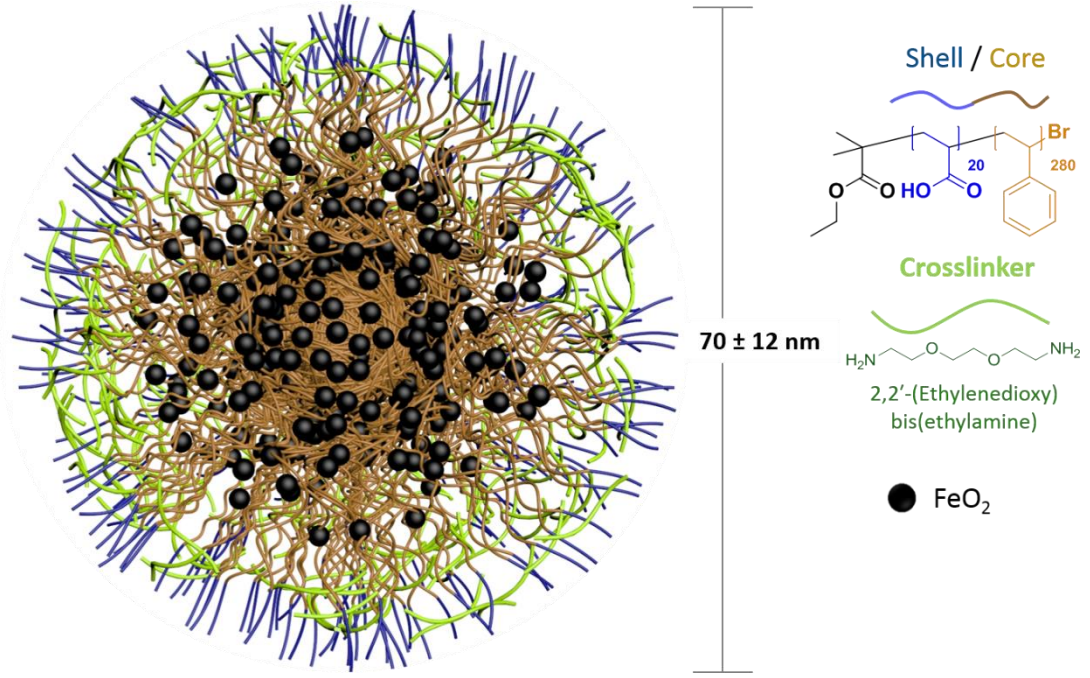

Figure 2 - Morphology of MSCKs

The iron oxide particles in the MSCKs core impart a can then be used to recover the loaded particles *via* the application of a sufficiently strong magnetic field. Experiments conducted by Pavia-Sanders *et al.* indicate that MSCKs have a maximum loading capacity of *ca.* 10 grams of crude oil per gram of MSCKs [18]. Furthermore, Pavia-Sanders *et al.* were able to demonstrate the recyclability of these MSCKs with no loss in loading capacity.

In addition, Pavia-Sanders *et al* also postulated that MSCKs could be fine-tuned to target specific contaminants *via* modification to the composition of the core and/or shell of the polymers, potentially leading to a contaminant-specific remediation technology for species such as PCBs, heavy metals, or fluorinated compounds.

2. LITERATURE REVIEW

2.1. Groundwater Contamination and Contaminants

Although substantial environmental remediation efforts have been conducted since the inception of environmental programs such as the Resource Conservation and Recovery Act (RCRA) and the National Priority List (NPL), the need for environmental remediation remains high. In 2004, the United States Environmental Protection Agency (USEPA) estimated that between $6-8 billion were spent annually on environmental cleanup efforts, and forecasted that this rate was sustainable for 30 to 35 years [19]. In 2014 alone, 6,800 confirmed underground storage tank releases were reported to the USEPA, bringing the total number of unresolved UST sites to 74,000 [20]. In addition to these UST sites, the NPL has grown to over 1,300 sites, of which 45% include groundwater contamination [21]. From 2009 to 2011, the number of decision documents issued by the USEPA which included *in situ* remediation of contaminated groundwater continued its rising trend, totaling 38% of all decisions. Of these decision, bioremediation and chemical treatment were components of 62% and 35% of all decisions respectively, with the most prevalent contaminants being RCRA 8 heavy metals (69% of all sites), volatile organic compounds (67%), and semi-volatile organic compounds (59%).

2.2. Current Groundwater Remediation Technologies

The predominant technologies currently employed for the remediation of groundwater include various combinations and permutations of chemical oxidation and reduction, biological degradation and natural attenuation, soil vapor extraction, and

immobilization *via* sorption media [22]. Each of these methods has limitations which must be considered when designing a remediation project.

2.2.1. Chemical Oxidation and Reduction

Chemical oxidation and reduction makes use of highly reactive agents such as hydrogen peroxide, permanganate, persulfate, or ozone to chemically transform pollutants into benign species *via* oxidation and reduction [23]. This process is typically conducted *in situ* and is commonly referred to as *in situ* chemical oxidation however *ex situ* chemical oxidation can also be conducted to treat aqueous phase contaminants. From 2009 to 2011, 82% of chemical treatments reported to the USEPA in decision documents were ISCOs [21]. Although effective, *in situ* chemical oxidation is not without risk; the highly reactive species used to remediate groundwater contamination are non-selective, which can result in much of the reactant being consumed by scavenger reactions [23, 24] or with the reactant interacting negatively with local geochemistry or subsurface utilities [23, 25, 26]. Additionally, the transformation of contaminants can also result in the generation of high temperatures and pressures which can result in surface eruptions [27]. Because these reagents are aqueous phase reagents, it has also been shown that treatment efficiency using *in situ* chemical oxidation is greatly diminished with increasing contaminant hydrophobicity, sorption [28, 29], and age [30]. Since both adsorption and diffusion are relatively slow processes when compared to oxidation/reduction and since both are concentration driven, the low levels of contaminants in the aqueous phase post-treatment will equilibrate with contaminated media and disconnected pore spaces. This equilibration results in the desorption of contaminants from the media and diffusion

of contaminants from dead volumes or non-aqueous phase liquids (NAPL) back into the primary flow channels, often causing contaminant levels in groundwater to "rebound" post treatment [23]. Because of this rebound effect, multiple applications may be necessary to achieve a stable concentration below the desired endpoint. To combat these problems, *in situ* chemical oxidation is often conducted in the presence of a surfactant or co-solvent which increases the solubility of hydrophobic species, thus increasing the efficiency of aqueous phase oxidants [29, 31].

2.2.2. Biological Degradation

Biological degradation is relatively inexpensive, self-regulating, and capable of treating contaminants in both the aqueous and sorbed phases. This has led to the increased popularity of biological degradation as a groundwater remediation technology; from 2009 to 2011, biological degradation was used in 62% of all USEPA records of decision [21]. Most bioremediation projects are conducted in anaerobic conditions (83%); however, aerobic bioremediations are not uncommon. Bioremediation has successfully been used to remediate a number of common environmental contaminants including petroleum hydrocarbons, methyl *tert*-butyl ether (MTBE), and halogenated compounds. Although often deployed with great success, biological degradation may be limited by the toxicity of the contaminant and the desired level of cleanup [32-34]. Biological systems are also sensitive to other factors such as dissolved oxygen, nutrient requirements, and pH, which can be problematic in some treatment scenarios. In addition to these limitations, biological degradation is relatively slow, when compared to chemical processes, and can take years to reach a stable endpoint [35]. Because of the kinetic

limitations on both the speed and the minimum level of contaminant concentration attainable, biological treatment is often used as a long term management strategy rather than a treatment strategy, which can require cost and man hour intensive long term monitoring and management [26, 34].

2.2.3. Soil Vapor Extraction

Soil vapor extraction (SVE) is a remediation method in which pressure and/or thermal gradients are established to drive the vaporization and collection of volatile and semi-volatile compounds [36]. These systems are very effective at rapidly decreasing contaminant levels in highly impacted areas; however, they are only applicable to contaminants which have high vapor pressure and low water solubility. Similarly to bioremediation, these systems can also take years to achieve endpoint goals [37].

2.2.4. Sorption Media

Sorption media are typically employed in either a pump and treat system or in permeable reactive barriers (PRBs). Sorption media remove contaminant by providing an energetically favorable surface to bind to, usually *via* the hydrophobic effect or surface charge [38, 39]. In addition to being able to physically sequester contaminants, *in situ* sorption media, such as PRBs, have been shown to promote biological degradation and/or catalytic reduction similar to what is observed in attached growth reactors [40, 41]. In these situations, the sorption media has the benefit of rapid and nearly complete contaminant removal coupled with an ongoing contaminant destruction process. Unfortunately, these systems tend to be difficult and expensive to deploy. Sorption systems are further limited in that they are only effective at treating water which flows

through them. Due to the fact that these systems are stationary, they are really only practical in situations where contaminated water can be diverted through them, such as in a funnel and gate PRB [39]. Although they are excellent systems for the treatment of ongoing groundwater contamination, such as the effluent from a landfill, sorption media are not appropriate for source treatment nor are they appropriate in areas where groundwater fluctuates or cannot be controlled, such as coastal areas or areas with large seasonal variations in groundwater gradient [40].

2.3. ENPs in a Groundwater Setting

Although aggregation and sorption act as barriers for most groundwater remediation applications, the injection of nZVI has been heavily investigated as means for remediating point source contamination and for use in PRBs [1, 42-44]. This interest is largely due to the fact that microscale ZVI has been used in this manner for quite some time, and conversion to nZVI improves upon all aspects of the existing process [7, 38, 39]. Although the mobility of nZVI remains limited to within a meter of the injection well head, the injection of nZVI slurries into wells can create PRBs at a fraction of the cost of traditional methods [7]. Additional work has been done to improve the transmissibility of nZVI through saturated porous media by reducing sorption and aggregation *via* surface modification of nZVI particles, however the success of these experiments was limited [15, 42, 45-48].

While nZVI has received the most attention, other existing remediation technologies have benefitted from conversion to nanoscale as well, including metal oxides, bimetallic particles, and sorbent materials, such as activated carbon, zeolites, and fullerenes [1,

[2].While much of the research regarding the application of ENP to environmental remediation has been focused on the miniaturization of existing technologies, the development of novel engineered nanomaterials remains limited. In the early 2000s, carbon based nanotubes and fullerenes were investigated as injectable sorption media due to their extremely high affinity for the adsorption of the organic contaminants such as petroleum or hydrocarbons [49]. With surface modifications, these same ENPs have also been shown to have a high affinity for heavy metals [50, 51]. Unfortunately, the cost of manufacturing these nanoparticles has historically prevented their industrial use for groundwater remediation, as have concerns about them acting as "Trojan horses". The Trojan horse effect has been observed when loaded carbon nanotubes are ingested and changes in the ambient environment such as pH and dissolved oxygen prompt the release of the contaminants from the ENP into the surrounding environment [52-55]. This same effect has also been observed with titanium dioxide [56]. In this case, it is not the ENP itself that is hazardous, but the contaminant which is being transported by the ENP.

Although several polymers have been investigated for the stabilization of nZVI, the application of novel polymeric ENPs for *in situ* groundwater remediation remains limited. A 2004 study by Tungittiplakorn *et al. (2004)* explored the use of amphiphilic polyurethane nanoparticles (APU) designed for the entrapment of polynuclear aromatic hydrocarbons (PAHs). Although removal of NAPL PAHs from a sand column was reported, particle transport was limited due to particle aggregation, and in some of the column studies, breakthrough was not observed.

2.3.1. Nanoparticles for Groundwater Remediation

Although aggregation and sorption act as barriers for most groundwater remediation applications, the injection of nZVI has been heavily investigated as means for remediating point source contamination and for use in PRBs [1, 42-44]. This interest is largely due to the fact that microscale ZVI has been used in this manner for quite some time, and conversion to nZVI improves upon all aspects of the existing process [7, 38, 39]. Although the mobility of nZVI remains limited to within a meter of the injection well head, the injection of nZVI slurries into wells can create PRBs at a fraction of the cost of traditional methods [7]. Additional work has been done to improve the transmissibility of nZVI through saturated porous media by reducing sorption and aggregation *via* surface modification of nZVI particles, however the success of these experiments was limited [15, 42, 45-48].

While nZVI has received the most attention, other existing remediation technologies have benefitted from conversion to nanoscale as well, including metal oxides, bimetallic particles, and sorbent materials, such as activated carbon, zeolites, and fullerenes [1, 2]. In the early 2000s, carbon based nanotubes and fullerenes were investigated as injectable sorption media due to their extremely high affinity for the adsorption of the organic contaminants such as petroleum or hydrocarbons [49]. With surface modifications, these same ENPs have also been shown to have a high affinity for heavy metals [50, 51]. Unfortunately, the cost of manufacturing these nanoparticles has historically prevented their industrial use for groundwater remediation, as have concerns about them acting as "Trojan horses". The Trojan horse effect has been observed when loaded carbon

nanotubes are ingested and changes in the ambient environment such as pH and dissolved oxygen prompt the release of the contaminants from the ENP into the surrounding environment [52-55]. This same effect has also been observed with titanium dioxide [56]. In this case, it is not the ENP itself that is hazardous, but the contaminant which is being transported by the ENP.

Although several polymers have been investigated for the stabilization of nZVI, the application of novel polymeric ENPs for *in situ* groundwater remediation remains limited. A 2004 study by Tungittiplakorn *et al. (2004)* explored the use of amphiphilic polyurethane nanoparticles (APU) designed for the entrapment of polynuclear aromatic hydrocarbons (PAHs) [57]. Although removal of NAPL PAHs from a sand column was reported, particle transport was limited due to particle aggregation, and in some of the column studies, breakthrough was not observed.

2.3.2. Nanoparticles as Emerging Contaminants

While some ENPs are completely benign, nanoparticle toxicity is not as simple as toxicity from soluble species. Some metal oxide and fullerene ENPs even have biphasic toxicological effects, with ENPs having a size threshold above which no effects are observed and below which LD_{50} concentrations of as low as 1 ppm have been reported [8]. Although the exact mechanism for this size dependent toxicity is unknown, the prevailing hypothesis is that ENPs below the biphasic threshold are able to penetrate the cell wall and cause acute toxicity effects within the interior of the cell. In contrast, many ENPs do not exhibit toxicity and some are even used as drug delivery systems [8, 9, 58, 59].

There are currently no nanotechnology specific contaminant levels established, due largely to the limitations related to detection, characterization, and risk assessment [8]. To overcome this hurdle, several federal agencies have devoted resources to researching the environmental and human health effects of ENPs. The National Nanotechnology Initiative has allocated over $575 million in environmental, health, and safety research related to nanotechnologies since 2008 [60]. In addition, the National Science Foundation , National Toxicology Program , National Institute for Occupational Safety and Health, Department of Defense, Department of Energy, and the USEPA have all created funding bodies for nanotechnology health and safety related research [61]. In 2010, the USEPA began recognizing nanomaterials as emerging contaminants and began developing a Significant New Use Rules which would require future manufacturers of ENMs to characterize these materials and declare them to the USEPA under the Toxic Substance Control Act [62]. Although maximum contaminant levels and maximum contaminant level goals have not yet been established for any ENPs, they have been established for their macroscale counterparts and the USEPA has jurisdiction under the Safe Drinking Water Act and the Clean Water Act to regulate ENP concentrations [63]. The vast majority of ENPs in industry, however, are in the personal care product and pharmaceutical industry which is regulated by the Food and Drug Administration.

2.4. MSCKs and their Potential Groundwater Remediation Applications

Although MSCKs have been shown to have excellent loading capacity in aqueous phase experiments, the application of these particles to a groundwater system has yet to be tested. However results reported by Pavia-Sanders *et al*. [18] indicate that MSCKs are a

promising candidate. The amphiphilic nature of the particles along with their size and suspension characteristics lend to a scheme in which MSCKs could be injected into one well head and later extracted from either the same well head or another well head, similar to current *in-situ* chemical oxidation injection schemes. MSCKs offer advantages over traditional ISCO in that they are non-reactive, meaning that there are minimal concerns pertaining to interactions with local geochemistry, subsurface utilities, or with the production of toxic intermediaries. Although exact sequestration kinetics were not reported in Pavia-Sanders *et al.*, the maximum loading capacity of the MSCKs was attained within 30 minutes, indicating that remediation using MSCKs would be much more rapid than bioremediation.

Additionally, Pavia-Sanders *et al* demonstrated that the MSCKs are recyclable with no loss in loading capacity, meaning that MSCKs may be a particularly cost-effective technology in situations where long-term management is necessary. Since this project is focused on determining the viability of MSCKs as a groundwater remediation technology, the cost of treating hydrocarbons using MSCKs was compared to the cost of treating hydrocarbons using the more traiditonal chemical methods (persulfate and Fenton's reagent). For the MSCKs, the maximum loading capacity reported by Pavia-Sanders *et al* was assumed, rending a reagent demand of 1 gram of MSCK per 10 g of hydrocarbon to be treated. For traditional chemical methods, reagent demand was calculated by summing the half reactions for the complete transformation of ethylene to carbon dioxide and water under base and ferric catalysis. For both Fenton's reagent and persulfate, initial pH was assumed to be natural. Reagent costs were taken from the

Sigma Aldritch and total treatment cost per gram of ethylene was summing the product of each reagents cost and stoichiometric coefficient. The resulting calculations indicate that MSCKs under ideal conditions have a treatment cost of 7.5¢ per gram of ethylene while persulfate and Fentons stoichiometrically estimated at 95¢ and $1.28 per gram of ethylene respectively. Although they may be cost effective, many potential barriers to the successful application of MSCKs for groundwater remediation are present.

First the results reported by Pavia-Sanders *et al.* (2013) represent ideal conditions which are not attainable *in situ*. The sequestration of weathered crude oil was accomplished by adding MSCKs to vials with free phase crude oil in the form of sheen. These vials were mixed to optimize MSCK and NAPL contact which greatly increase contact between the crude oil and the MSCKs. While some mixing does occur *in situ* due to dispersion, it is not nearly to the level in of the experimental methodology reported by Pavia-Sanders *et al* (203).

Second, particle aggregation, both with other MSCKs and with other particulates, was not a consideration for Pavia-Sanders *et al*. In groundwater systems, particle aggregation reduces transmission of MSCKs *via* pore clogging and can reduce the overall effectiveness of the MSCKs.

The effects of pH and salinity on the morphology and efficiency of MSCKs is also unknown as are the sequestration and release kinetics of MSCKs. Although contact time of around 30 minutes was sufficient to yield the optimal loading capacity reported by Pavia-Sanders *et al*, it is unknown if the sequestration of aqueous phase and NAPL contaminants during transport will be kinetically limited. Furthermore, loaded MSCKs

have not been tested in pristine aqueous phase to determine if sequestered contaminants are released. This is of particular concern given the behavior of sorption based ENP such as fullerenes, in which the particles themselves are non-toxic, but loaded particles can induce acute toxicity effects when desorption occurs.

Regarding toxicity, it should also be noted that similarly structured ENPs have been used for a variety of biomedical applications such as drug delivery systems and contrast agents for medical imaging, and are safe for injection or ingestions [64]. Although MSCKs have not yet undergone toxicity testing, tests of MSCKs in zebra fish and/or worms are planned but have not yet been published

2.5. Modeling ENP Transport

ENP adsorption and retention in saturated porous media has been well studied for a variety of carbon based, metal, and metal oxide ENPSeg: [17, 65, 66-72]. These studies have found that the sorption and retention of ENPs behave somewhere between soluble species and macroscale colloidal suspensions. The sorption and retention of ENPs is controlled by four major properties: flow velocity [73, 74], ENP surface charge (zeta potential) [75], ionic strength of the water [65], and the presence of organic species [76]. There are currently numerous competing numerical models available to describe particle transport, most of which are adapted from bacterial and viral transport models [77-82]. In general, these numerical models fall into one of two groups: those based on colloidal filtration theory and those using kinetic attachment and detachment equations (Table 2). In general, these models seek to predict both particle transport behavior and particle deposition and retention in saturated porous media. Unfortunately, existing models tend

to have low predictability when size effects and aggregation are present [17, 65, 66, 72]. Classically, ENP transport is modeled colloidal filtration theory (CFT) as would be modeled for macro scale colloidal suspensions. Although this method can yield reliable results for some larger ENPs, as the size of the ENPs decreases, the significance of atomic effects on the sorption and retention of the ENPs increases and classical CFT fails to account for these interactions. To overcome this, several researchers have attempted to supplement CFT with the Derjaguin – Landau – Verwey − Overbeek (DLVO) theory with varying degrees of success [65, 83, 84]. Not surprisingly, the results of these studies indicate that larger ENPs generally have a higher retention in saturated porous media, however until the effects of particle size, molar concentration, and aggregation on ENP retention and transport can be quantified, the development of a numerical model is likely to be confounded. There are even examples of DLVO modified CFT being applicable to 52 nm silica ENP, but not to 8 nm particles prepared under identical conditions [65].

In contrast to CFT which was adapted from micro scale colloidal transport modeling, kinetic modeling is an adaptation of soluble species transport which is adapted for discrete particles. A 2014 study by Goldberg *et al* assessed over 100 ENP column studies from the last decade and found that, in general, kinetic models tend to have better predictive power than CFT models [85]. However, they also cautioned that current iterations of both CFT and kinetic models currently being employed to predict ENP transport are unsuitable for a broad range of ENPs. They found that while current particle transport models could successfully duplicate measured breakthrough curves,

they performed poorly with regards to particle deposition. Goldberg *et al.* concluded that the mechanisms governing nanoparticle fate and transport in saturated porous media remain ill-defined and that the suitability of current ENP transport models is questionable.

Table 2 – Particle transport models (adapted from Goldberg *et al.*).

	Governing Mass Balance	Type	Supporting Mass Balance Equations
Colloidal Filtration Theory	$\frac{\partial C}{\partial t} = -v_p \frac{\partial C}{\partial x} - \frac{\rho_b}{\theta}\frac{\partial S}{\partial t}$	Single Deposition Mode	$\frac{\rho_b}{\theta}\frac{\partial S}{\partial t} = k_d C$ $k_d = \frac{3(1-\theta)}{2d_c}\alpha v_p \eta_{eff}$
		Dual Deposition mode	$\frac{\rho_b}{\theta}\frac{\partial S}{\partial t} = f k_{d1} C + (1-f) k_{d2} C$ $k_{d1} = \frac{3(1-\theta)}{2d_c}\alpha_1 v_p \eta_{eff}$ $k_{d2} = \frac{3(1-\theta)}{2d_c}\alpha_2 v_p \eta_{eff}$
Kinetic Attachment and Detachment	$\frac{\partial C}{\partial t} = D_p \frac{\partial^2 C}{\partial x^2} - v_p \frac{\partial C}{\partial x} - \frac{\rho_b}{\theta}\frac{\partial S}{\partial t}$ $D_p = \frac{D}{\tau} + \alpha_L v_{NP} * \frac{(\partial^2 C)}{\partial x^2}$	Single Site Deposition and Remobilization	$\frac{\rho_b}{\theta}\frac{\partial S}{\partial t} = k_d C - \frac{\rho_b}{\theta} k_r S$
		Dual-site Deposition Remobilization	$\frac{\partial S}{\partial t} = \frac{\partial S_1}{\partial t} + \frac{\partial S_2}{\partial t}$ $\frac{\rho_b}{\theta}\frac{\partial S_1}{\partial t} = k_d C - \frac{\rho_b}{\theta} k_r S$ $\frac{\rho_b}{\theta}\frac{\partial S_2}{\partial t} = k_{d,2} C - \frac{\rho_b}{\theta} k_{r,2} S$
		Langmuirian Blocking	$\frac{\rho_b}{\theta}\frac{\partial S_1}{\partial t} = k_d \psi_b C - \frac{\rho_b}{\theta} k_r S$ $\psi_b = \left(1 - \frac{S}{S_m}\right)$
		Depth-Dependent Retention	$\frac{\rho_b}{\theta}\frac{\partial S_1}{\partial t} = k_d \psi_s C - \frac{\rho_b}{\theta} k_r S$ $\psi_s = \left(\frac{d_c + x}{d_c}\right)^{-\beta}$

α: attachment efficiency[-]; α_L: intrinsic dispersivity [m]; β: empirical depth dependent retention parameter [-]; C: suspended ENP concentration [kg m^{-3}]; D: molecular diffusion coefficient [m s^{-1}]; D_p: hydrodynamic dispersion coefficient [m s^{-1}]; f: particle population fraction associated with α [-]; k_d: deposition rate constant [s^{-1}]; k_r: remobilization rate constant [s^{-1}]; η_{eff} : effective porosity [-]; ψ_b: langmuirian blocking coefficient [-]; ψ_s: depth dependent retention function [-]; S : solid phase concentration [kg$_{ENP}$ kg$_{Soil}^{-1}$]; S_m : maximum solid phase concentration [kg$_{ENP}$ kg$_{Soil}^{-1}$]; τ : tortuosity [-]; t: time [s]; v_p: pore water velocity [m s^{-1}]; v_{NP}: mean particle velocity [m s^{-1}]; x: distance from column inlet [m];

3. EXPERIMENTAL METHODS AND MATERIALS

Because the goal of this project is to assess the viability of MSCKs as a groundwater remediation technology, methods and materials are reflective of conditions which would be encountered during a groundwater remediation. As such, column characteristics are reflective of aquifers in which induced flow is possible and therefore injection is viable.

3.1. Selection of Porous Media

When conducting ENP transport studies, glass beads and quartz sands are commonly used as saturated porous media [86]. Although this is common practice, sand and glass beads have much less potential to interact with ENP or soluble species than clays [87]. In order to allow for a full range of interactions, two types of porous media were used in this study: Texas Gold 40/70 sand (FTS International, Houston, Tex.) and kaolin clay (Sigma Aldrich, St. Louis, Mo.).

Sand used in this project was mined in Voca, Texas from the Hickory formation, a minor aquifer in central Texas, and is representative of sand present in an aquifer. Sphericity, roundness, acid solubility, bulk density, and specific gravity are all reported

Table 3 - Properties of Texas Gold sand

Sphericity [-]	**Roundness [-]**	**Acid Solubility [%]**	**Bulk Density [g cm^{-3}]**	**Specific Gravity [g cm^{-3}]**
>= 0.6	0.8	1.1	1.46	2.63

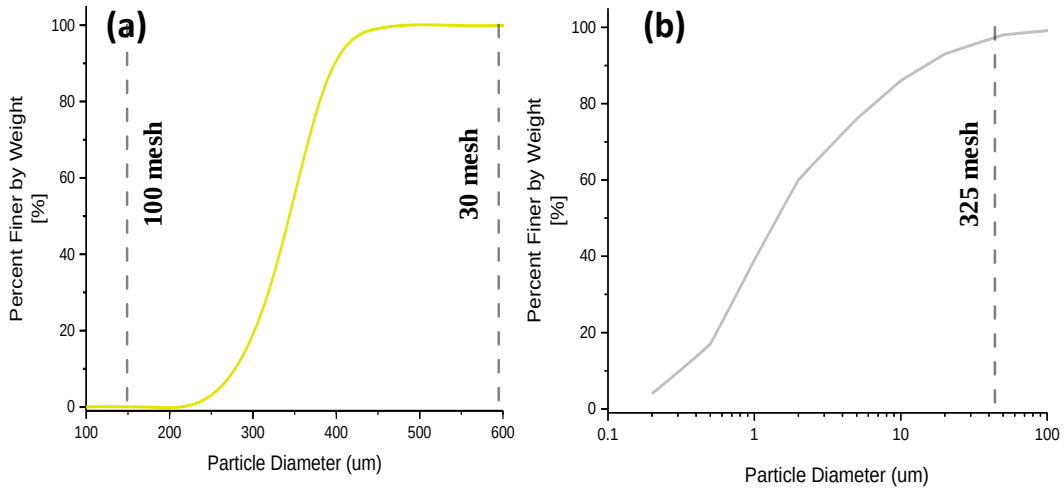

Figure 3 - Grain Size distribution for (a) Texas Gold sand (adapted from *FTSI International*) and (b) kaolin clay (adapted from Murray 2008 and Conley 1966).

by the manufacturers and are summarized in Table 3 [88]. Particle size distribution was determined by sieve analysis and was conducted by the manufacture (Figure 3a).

Kaolin clay was selected because it is a readily available, non-expansive earth clay [89]. These clays are derived from weathered granites, gneisses, and phylites and were commonly deposited in still water areas such as lagoons, estuaries, oxbows, lakes, and ponds during and are prevalent in Georgia and South Carolina. They have a dual layer crystalline structure comprised of silica oxide and aluminum oxide. Although the grain size distribution was

not reported by the manufacturer, their particle size distribution is fairly well known (Figure 3b) [89, 90].

In each treatment one of two porous media mixtures was selected: 100% sand or 90.5% sand and 9.5% clay. The 100% sand columns were used in experiments to

represent ideal conditions, whereas the sand/clay columns provide additional surfaces for MSCKs to interact with during transport and are meant to represent a simulated aquifer soil. Sand/clay mixtures were homogenized *via* vigorous mixing prior to use in any column experiments.

3.2. Simulated Contaminant Selection

Pavia-Sanders *et al*. reported sequestration of weathered crude oil with no preferential sequestration for specific hydrocarbons [18]. In order to adequately differentiate between sequestration of aqueous phase contaminants and non-aqueous

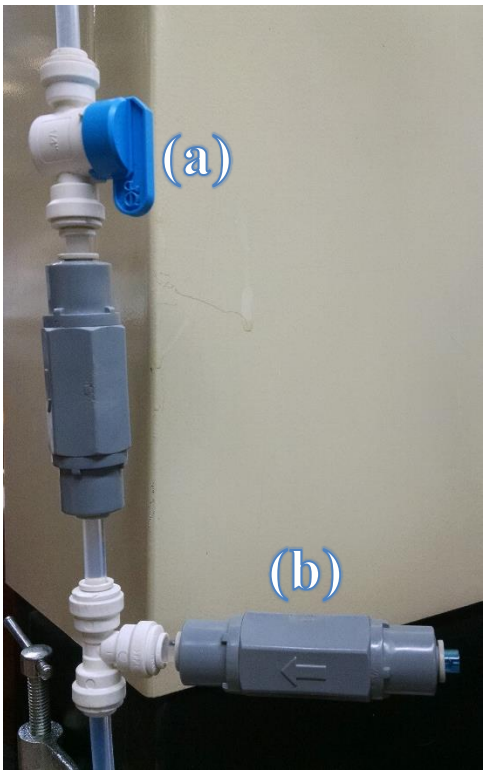

Figure 4 – Column injection manifold. (a) Constant head permeameter feed valve . (b) Injection check valve.

phase contaminants, two simulated contaminants were selected for this study: *m*-xylene for aqueous phase contamination and mineral oil for non-aqueous phase contamination. Although hydrocarbons tend to have low solubility in water, *m*-xylene was selected due to its prevalence as an environmental contaminant, its relatively high solubility (161 mg/L), and its relatively high Tier 1 protective concentration level (10 mg/L) [91, 92]. Mineral oil was selected due because of its availability, low solubility, and non-volatile nature.

The contaminated aqueous phase consisted of an 8.66 mg/L *m*-xylene solution which was prepared in 20 L batches. This *m*-xylene solution was used as the influent aqueous phase for columns in which aqueous phase contamination was necessary. The introduction of free phase contamination was accomplished by the addition of mineral oil during the packing of the columns. This was done by the addition of 200 ml of mineral oil on top of the standing water during the wet packing of the columns (see Section 3.4 for details pertaining to the wet packing procedure). This addition of mineral oil to the wet packing process allowed for the formation of free phase pockets within pore spaces of the porous media during the loading process

3.3. Non-reactive Tracer Selection

Bromide (Br^-) was selected as a non-reactive tracer and was used to characterize each of the columns prior to the addition of MSCKs. Tracer test were conducted a minimum of five times for each column and were conducted *via* the injection of 10 ml of Br^- solution into the injection check valve (Figure 4b). Effluent concentration was then

monitored The Br^- tracer was prepared via the addition of potassium bromide to nanopure water.

3.4. Column Parameters and Loading

Columns used in this study were 5 inches in diameter and 24 inches in length and were made of aluminum (Soil Moisture Equipment Corp Y1250L24-B0.5M2) (Figure 5). Endplates were attached to either end of the column screened using 325 mesh screen. Porous media was loaded into the columns using standard wet packing methods, wherein the porous media was added into 1-2 inches of standing water, with additional water being added to maintain a constant standing water level [93]. During the loading of columns, the sides of the column were tapped using a hammer to ensure uniform and consistent settling of the media. During the loading of sand/clay columns, the porous media was stirred every 6 inches to minimize the formation of air bubbles. For each column, the dry mass of porous media added was measured and recorded.

3.5. Injection Schemes

The introduction of Br– and MSCKs into the columns was accomplished via the injection manifold located between the column influent and the permeameter. To approximate an instantaneous pulse, each injection was preceded by the closing of the permeameter feed valve (Figure 4a), followed by 10 ml of the MSCKs or Br – solution into the injection check valve via syringe (Figure 4b). Next, the injection check valve was purged and the MSCK or Br – solution was transported past the injection manifold t-joint by a 10 ml injection of feed solution from the reservoir *via* syringe. Once the injection check valve was purged, the feed valve was re-opened and the run was started.

The goal of this injection scheme is to approximate an instantaneous pulse of injected material while minimizing mixing due to introduction into the flow stream prior to the column influent. Additionally, this injection scheme minimizes injection

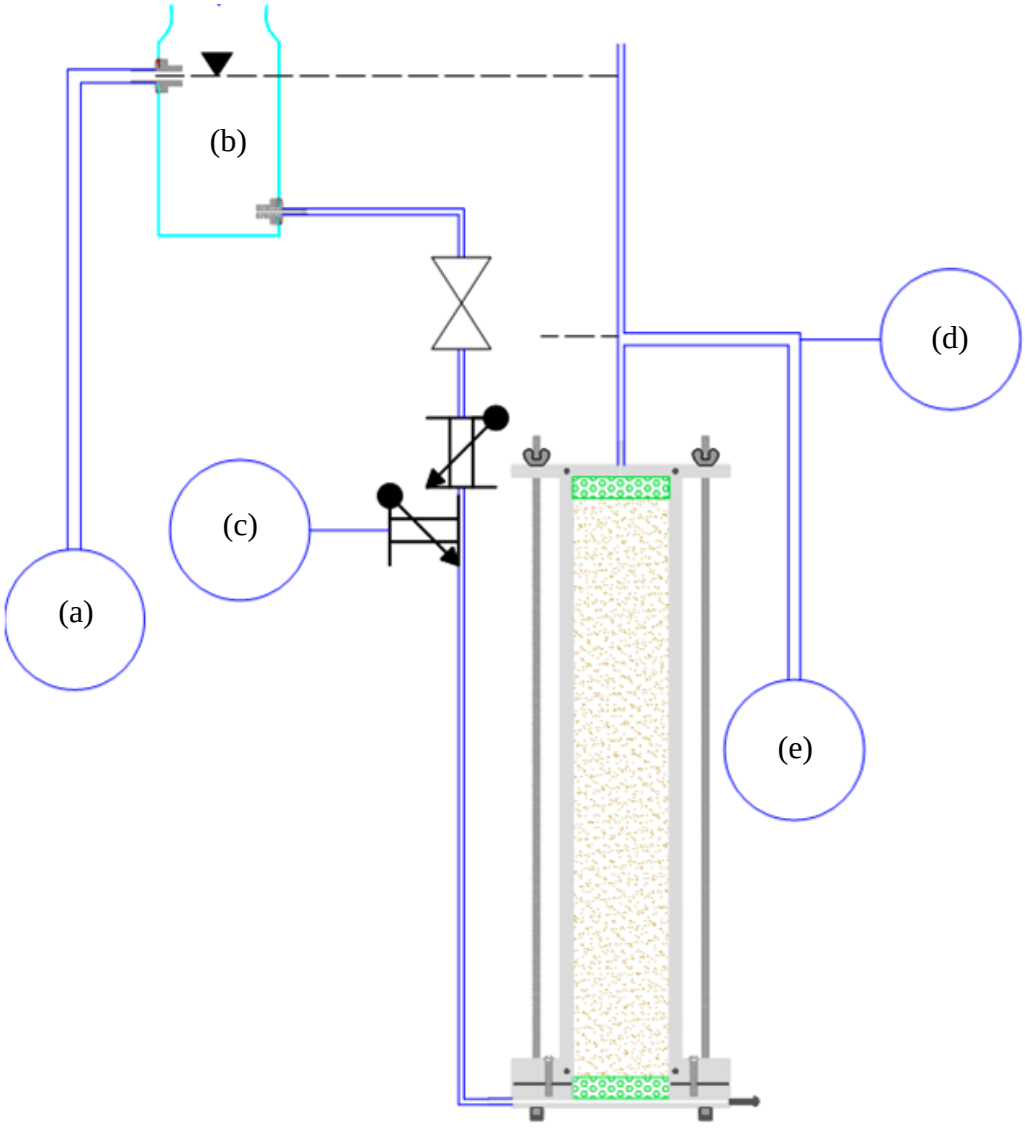

Figure 5 - Column Setup. (a) Feed reservoir (b) constant head permeameter (c) injection port (d) detector (e) waste line.

inefficiencies and losses due to residual injection solution within the check valve or before the t-intersection, and front mixing caused by the proximity of the CHP feed valve to the injection point.

3.6. Column Influent and Effluent Control

Water flow was controlled *via* the use of a constant head permeameter (CHP) (Figure 5b). Flow into the CHP was controlled *via* a peristaltic pump (Geotech Geopump) which was fed from a water reservoir consisting of micropure water or an 8.66 mg/L *m*-xylene solution. Overflow from the CHP was re-routed back into the reservoir. The influent column flow rate was controlled by controlling the elevation head between the CHP and column effluent *via* the raising or lowering the CHP, with volumetric flow rates ranging from 2.5 mL/s to 5.3 mL/s and the head difference ranging from 59 cm to 160 cm.

Column effluent was routed through a t-intersection with an open vertical shaft (Figure 5f) and a waste feed line (Figure 5e). Effluent flow rate was calculated by routing the column effluent to a graduated cylinder and measuring the amount of time required to reach the 500 ml mark. Flow rate was measured in this manner at the start, mean residence time (MRT), and end of each run (Figure 6). Effluent sampling was conducted in two ways: manually and automatically. Manual sample collections were completed by routing the effluent into sample containers. Automatic effluent sampling was accomplished via the withdrawal of a portion of the effluent from the open top segment of the effluent t-intersection using a “super sipper” peristaltic pump (Figure 5).

3.7. Media Characterization

The characteristics of the saturated porous media were determined for each column. Hydraulic conductivity was determined *via* CHP test by measuring the amount of time (*t*) required for the effluent to fill a 500 ml volume (*V=500 ml*), given the length of the column (*L = 60.96 cm*) and the cross sectional surface area of the column (*A=506.7 cm*^{2}) [93].

$$K_t = \frac{V * L}{A * t * H}$$

Effective porosity was calculated by taking the MRT of Br^- in the conservative tracer tests and multiplying by the volumetric flow rate (*Q*) to yield the pore water volume of the columns (V_w). This volume was then divided by the total volume of the column (V_T) to yield the effective porosity

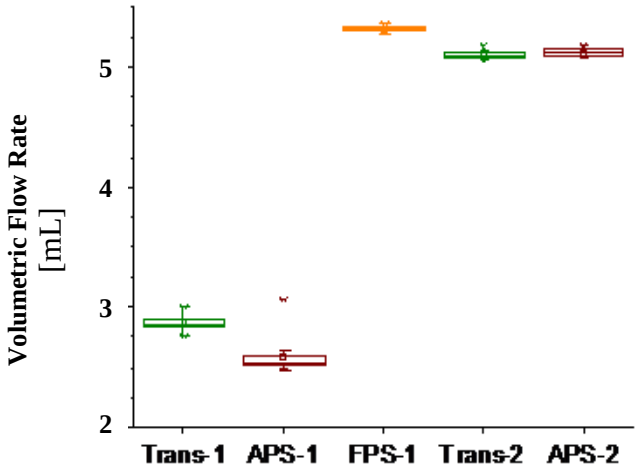

Figure 6 - Volumetric flow rates for each column

$$\eta_{eff} = \frac{V_w}{V_T}$$

$$V_w = Q * MRT_{Br}$$

$$V_T = A * L$$

Intrinsic dispersivity (α_L) was calculated *via* the fitting of transport parameter values to measured Br^- breakthrough curves through least square regression using the one-dimensional advection dispersion equation under the assumptions that dispersion is much greater than molecular diffusion and that Br^- is conservative:

$$\frac{\partial C}{\partial t} = D_p \frac{\partial^2 C}{\partial x^2} - v_p \frac{\partial C}{\partial x}$$

$$D_p = \alpha_L v_p * \frac{(\partial^2 C)}{\partial x^2}$$

3.8. Detection and Quantification of Effluent Concentrations

Effluent Br^-, MSCK, *m*-xylene, and mineral oil concentrations were monitored using UV-visible spectroscopy. Initial experiments were conducted using a single beam deuterium/tungsten lamp Helios Gamma UV-Vis Spectrophotometer; however, contaminant sequestration experiments were later duplicated using a dual beam Shimadzu UV-2550 due to the need to measure absorbance at multiple wavelengths during a single run. The capabilities of both spectrophotometers are summarized in Table 4.

Table 4 – Spectrophotometric capabilities of the Helios Gama and the Shimadzu UV-2250

	Helios Gama	**Shimadzu UV-2250**
Wavelength range [nm]	190 — 1100	190 — 1100
Wavelength accuracy [nm]	±1	±0.3
Wavelength repeatability [nm]	±0.2	±0.1
Resolution [nm]	0.5	0.1
Photometric accuracy @ 1 Abs [Abs]	±0.005	±0.004
Photometric repeatability @ 1 Abs [Abs]	±0.002	±0.002

4. TRANSPORT, CHARACTERIZATION, AND MODELING OF POLYMERIC NANOPARTICLES ENGINEERED FOR THE SELECTIVE ENTRAPMENT AND RECOVERY OF CONTAMINANTS IN SATURATED POROUS MEDIA

4.1. Synopsis

One-dimensional impulse column experiments of monodisperse magnetic shell crosslinked knedel-like nanoparticles (MSCKs) were conducted to investigate the transport, retention, and sequestration of hydrophobic pollutants in saturated porous media. Solutions of well-suspended monodisperse MSCKs were injected into water saturated columns packed with either sand or a sand/clay mixture and operated under steady flow conditions. The effluent of these columns was monitored using UV-visible spectroscopy to produce breakthrough curves of the MSCKs, aqueous phase contaminants, and a non-reactive bromide tracer. MSCKs were found to readily transport through sand with a 99% recovery. In the presence of clays, recovery was reduced to 63%. The presence of both aqueous phase contaminants further reduced the recovery of MSCKs to 61% in sand and 53% in clay; however, the MSCKs which were eluted had sequestered aqueous phase *m*-xylene to below the detection limit. Trials with the sequestration of non-aqueous phase contaminants were less successful, with only 52.5% recovery of the MSCKs and no detectible sequestration of mineral oil by the MSCKs. These initial results indicate that MSCKs may be an appropriate remediation technology for groundwater contamination; however, free phase contaminants currently pose a limitation. More work may be warranted to improve the transmission and interaction of

MSCKs with free phase contaminants by manipulating their chemical and morphological properties.

4.2. Introduction

Recently, engineered nanoparticles (ENPs) have been of particular interest to the environmental industry, both as a means of improving existing remediation technologies and as a potential emerging contaminant [94, 95]. The distribution and stabilization of nanoscale zero valent iron (nZVI) has been of particular interest [1, 42-44]. However, other studies have examined nanoscale versions of existing remediation technologies such as metal oxides, bimetallic particles, and sorbent materials, such as activated carbon, zeolites, and fullerenes, which have been investigated for their enhanced chemical and/or biological remediation effectiveness relative to their microscale counterparts [1, 2]. While the effectiveness of these technologies has been improved by conversion from the microscale to the nanoscale, field studies showed that the delivery of these nanoscale versions of traditional materials, such as nZVI, in the subsurface *via* injection is limited to within a few meters from the point of injection [7]. Thus, distribution of ENPs in the subsurface represents a major challenge in the commercial application of ENP for *in situ* groundwater remediation.

To improve the transport of nZVI, several surface modifications and coatings have been proposed and studied, predominantly hydrophilic polymers, however the transport of these surface modified ENPs remains limited [15, 46-48]. Although several polymers have been investigated for the stabilization of nZVI, the application of novel polymeric ENPs for *in situ* groundwater remediation remains limited. Tungittiplakorn *et*

al. (2004) explored the use of amphiphilic polyurethane nanoparticles (APU) designed for the entrapment of polynuclear aromatic hydrocarbons (PAHs). Although removal of non-aqueous PAHs from a sand column was reported, particle transport was limited due to particle aggregation, and in some of the column studies, no particle elution was detected.

The Deep Water Horizon oil spill in 2010 renewed interest in the development of novel surface water recovery technologies, particularly in the nanotechnology field. While much of this research has focused on the use of macroscale products comprised of nanoparticles (*e.g.*, foams [96] , hydrogels [97-99], sponges [100, 101]) several standalone ENPs have been identified as potential candidates for adaptation to *in-situ* groundwater remediation [18, 102, 103].

The most promising of these candidates are magnetic shell crosslinked knedel-like nanoparticles (MSCKs) produced by Pavia-Sanders *et al.* [18] [18]. These ENPs are comprised of micellized amphiphilic diblock copolymers of poly acrylic acid (PAA) and poly styrene (PS) with entrapped oleic acid-stabilized iron oxide nanoparticles in the core. These micelles were then crosslinked to stabilize the particles in aqueous environments. The MSCKs were tested using a highly complex contaminant, weathered crude oil, and were shown to have a maximum loading capacity of 10 grams of oil per gram of MSCKs, with no detectible preferential sequestration of specific components. Although initially designed for the recovery of hydrocarbon sheens, MSCKs have a number of attributes which make them attractive candidates for *in situ* groundwater

remediation and which set them apart from traditional *in situ* chemical remediation technologies:

1) MSCKs are non-reactive, meaning byproducts of chemical processes such as heat, pressure, and the generation of chemical species from scavenger or incomplete reactions are not a concern as they can be with chemical oxidation techniques such as Fenton's, persulfate, or iron oxide;

2) MSCKs are magnetically separable from the aqueous phase and recyclable, thus minimizing wasted MSCKs and waste generation; and

3) The crosslinked, amphiphilic morphology of the MSCKs function in much the same way that surfactants do, but exist as discrete particles rather than as a solution, thus allowing access to the enhanced transport and desorption properties of a surfactants within a controlled and discrete environment.

While MSCKs are an attractive candidate, the behavior of these ENPs in saturated porous media is unknown. Based on the morphology and surface characteristics of MSCKs, minimal interaction is anticipated between MSCKs and saturated porous media. However, mass loss and retention are a possibility, particularly when considering that particle aggregations was observed in benchtop experiments by Pavia-Sanders *et al* [18]. The purpose of this study is to explore the transport and contaminant sequestration behavior of MSCKs in saturated porous media to determine if these ENPs are a viable groundwater remediation technology candidate.

When discussing the transport of ENP in saturated porous media, it is important to note that there are currently multiple competing theories attempting to predict ENP

transport and retention in saturated porous media (*e.g.* colloidal filtration theory (CFT) [104], two site kinetic models [79], single site kinetic models with or without Langmuirian blocking and/or depth dependent retention [105, 106]). Although hundreds of column studies have been conducted over the last decade, the mechanisms governing nanoparticle fate and transport in saturated porous media remain ill-defined [85]. Unfortunately, the predictability and suitability of the models currently being employed varies drastically depending on the size and type of particles being studied and in some cases, none of the models are appropriate [85].

4.3. Materials and Methods

4.3.1. Preparation of MSCK Solution

MSCK solutions were produced stepwise using the methods previously outlined by Pavia-Sanders *et al.* Briefly, the methods are as follows:

4.3.1.1. Synthesis of diblock copolymer

PAA_{20}-*b*-PS_{200} was synthesized using the methods described in Davis *et al.*[107]. A diblock copolymer precursor was synthesized *via* sequential atom transfer radical polymerization (ATRP), first of *tert*-butyl acrylate followed by the subsequent polymerization of styrene in the presence of CuBr and *N,N,N',N'',N''*-pentamethyldiethylenetriamine at 55°C and 95°C, respectively. The final amphiphilic diblock copolymer, PAA_{20}-*b*-PS_{200}, was achieved by the removal of the *tert*-butly groups from the precursor *via* acidolysis in the presence of trifluoroacetic acid in dichloromethane.

Table 5- Column loading and flow conditions for MSCK transport experiments

Column	Treatment	Sand Content [%]	Clay Content [%]	$C_{m\text{-}xylene(aq)}$ [mg/L]	S_{water} [-]	S_{NAPL} [-]	q [a] [m/day]	v_p [b] [m/day]
S-1	Trans-1	100	-	-	1	-	19.6±0.9	39.0±1.7
S-1	APS-1	100	-	8.66	1	-	17.4±0.6	34.7±1.3
S-2	FPS-1	100	-	-	0.979	0.031	36.3±0.3	76.2±0.6
SC-1	Trans-2	90.5	9.5	-	1	-	34.9±0.4	81.9±0.9
SC-1	APS-2	90.5	9.5	8.66	1	-	34.4±1.0	80.7+2.3

[a] Darcy Velocity. [b] Average Linear (or Pore Water) Velocity.

4.3.1.2. Synthesis of iron oxide nanoparticles

Iron oxide nanoparticles were produced *via* the thermolysis of iron (III) acerylacetonate in the presence of 1,2-hexadecanediol in benzyl ether [108, 109]. Oleic acid and oleylamine were selected as the surfactant and co-surfactant respectively. The thermolysis was conducted over three consecutive 1-hr periods at 140, 200, and 250 ^{o}C. After cooling, the iron oxide nanoparticles were then precipitated in ethanol.

4.3.1.3. Micelle assembly and crosslinking

The magneto-micelles were formed using the methods outlined in Pavia-Sanders *et al.*[18] PAA_{20}-*b*-PS_{200} and iron oxide ENPs were suspended in a 1:1 by volume dual solvent mixture of *N*,*N*-dimethylformamide and tetrahydrofuran at a concentration of 0.33mg/mL for both inorganic and organic components. This mixture was then added drop wise to 0.15 eq. of nanopure water at a rate of 20 ml/h during simultaneous drop wise addition of nanopure water at the same rate. The resulting solution was then filtered through a 5 μm filter and dialyzed over 24 hours in nanopure water to remove excess

organic solvent. The micelle solutions were created in five batches and then combined prior to crosslinking to ensure homogeneity. Crosslinking was achieved *via* amidation by (2,2'-ethylenedioxy)bis(ethylamine) in the presence of 1-(3-(dimethylamino)propyl)-3-ethyl-carbodiimide methiodide. Dialysis in nanopure water was repeated after crosslinking to remove unreacted molecules and byproducts from the MSCK solution. The structure and size of the MSCKs was confirmed using transmission electron microscopy (TEM) (Figure 7a) and dynamic light scattering (DLS) (Figure 7b) with DLS reporting a mean particle diameter of 70± 12 nm. TEM analysis of over 80 particles yielded a mean particle diameter of 75± 30 nm. The concentration of the stock solution of MSCKs was determined in quintuplicate *via* the lyophilization of 5 ml solutions of MSCK and subsequent mass measurements using a microbalance, yielding a stock MSCK concentration of 216 mg/L.

4.3.2. Porous Media

Texas Gold 40/70 sand (FTS International, Houston, Tex.) and kaolin clay (Sigma Aldrich, St. Louis, Mo.) were selected as the porous media for this study. Grain size distribution, sphericity, roundness, acid solubility, bulk density, and specific gravity were all reported by the manufacturers and are available in the supplemental information (SI). Sand grain diameter averaged 207 microns, with an inner quartile range of 210 to 420 microns (see Figure 3).

4.3.3. Column Apparatus

The column was comprised of a 12.7 cm diameter and 61 cm long aluminum cylinder, and column end-plates were fitted with 325-mesh steel screens. For each

treatment, porous media was wet-packed in 2 inch increments. Upward flow was induced using a constant head permeameter.

4.3.4. Column Experiments

Five column treatments were used to characterize the transport and retention of MSCKs and the sequestration of hydrocarbons during transport (Table 5). Treatments Trans-1 and Trans-2 were used to determine baseline transport properties of MSCKs in sand (C1) and in a sand/clay mixture (C3) with pristine aqueous and solid phases. Aqueous phase sequestration (APS) Treatments APS-1 and APS-2 repeated treatments Trans-1 and Trans-2 with the introduction of *m*-xylene as an aqueous phase contaminant (8.66 mg/L *m*-xylene) by replacing the feed reservoir with an *m*-xylene. APS-1 and APS-2 were used to determine the effects of aqueous phase sequestration of

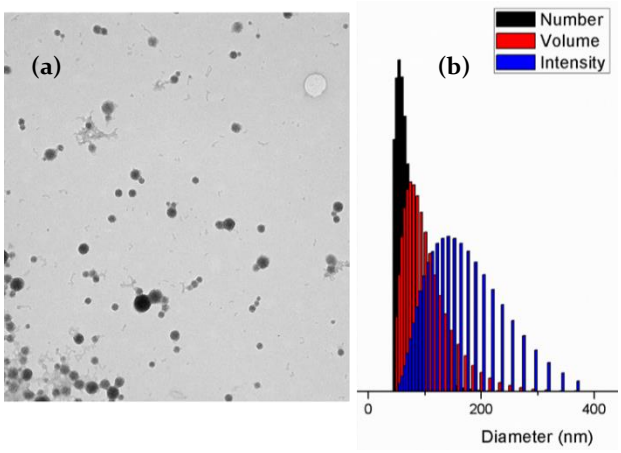

Figure 7- Characterization of MSCKs. (a) TEM of MSCKs drop deposited from water onto a Formvar grid (not stained); (b) number-, volume-, and intensity-averaged DLS histograms of MSCKs in water.

hydrocarbons on the transport properties of MSCKs. Free phase sequestration (FPS) Treatment FPS-1 was conducted in C3 and duplicated the conditions of Trans-1 with the introduction of a free phase liquid in the form of mineral oil. FPS-1 was used to determine the effects of MSCK/NAPL interactions on particle transport and to determine the MSCKs efficacy of NAPL sequestration during particle transport. Each treatment was repeated 5 times in order to determine the variability of the results, for a total of 25 column runs.

4.3.5. Detection and Quantification

A fraction of the column effluent was routed through a flow-through cell and monitored using UV-vis spectroscopy to produce absorbance breakthrough curves (BTC). Measured absorbance was converted to concentration using the Beer-Lambert law which states that absorbance (A) of a given species is a function of the path length traveled by the radiation (b), and the concentration (C) and molar absorptivity coefficient (ε) for the given species. Since ε is also a function of λ, the total absorbance of *m* species can be described by the summation:

$$A(\lambda)_{obs} = \sum_{n=1}^{m} C_n * b * \epsilon(\lambda)_n$$

When *m*=1, such as when the only absorbing species present is MSCKs, absorbance can be directly converted to concentration. When multiple absorbing species such as both MSCKs and *m*-xylene $_{(aq)}$ are present, absorbance is measured at an *m* different wavelengths, resulting in a system of linear equations which can be solved for the concentration of each species. Target wavelengths were selected based on the number of absorbing species present (one or two) and initial testing. Wavelengths used

as part of this study were 191.5 nm (for the Br^- tracer), 244 nm (local maximum for the styrene peak of the MSCKs), 212 nm (local maximum for acrylic acid peak), 273 nm (local maximum for *m*-xylene), and 206 nm (local maximum for mineral oil).
Prior to each experiment, the column was thoroughly flushed with micro pure deionized water (μDIW) until the effluent UV-vis readings stabilized.

4.3.6. Conservative Tracer Test

Prior to injection of MSCKs, each column was characterized *via* the injection of a non-reactive tracer. A treatment consisting of a 10 ml pulse of 207 mg/L KBr (Sigma Aldrich) was injected and column effluent was monitored using UV-vis. The resulting non-reactive tracer BTCs for bromide were fit to a 1-dimensional advection-dispersion model to determine the media characteristics of each column. Pore water velocity and Darcy velocity did not exceed 82.95 m/day and 35.34 m/day respectively (Table 5), yielding a maximum Reynolds number of 1.2 x 10-4. Porosity (η) was calculated from the Br^- BTC using the average volumetric flow rate (Q) along with the average mean residence (MRT) and total volume of the column (V_t):

$$\eta = \frac{MRT * Q}{V_t}$$

4.3.7. MSCK Transport and Retention Characterization

MSCKs were introduced to the column *via* a 10 ml pulse injection at the base of the column. In order to approximate instantaneous injection, flow to the columns was halted *via* the closing of the permeameter feed valve prior to the injection point. MSCKs were then injected followed by a 10 ml purge injection of background aqueous phase.

After both the injection and the purge were completed, the CHP valve was re-opened and monitoring of the effluent commenced. Effluent concentrations were recorded at intervals ranging from 4 to 6 seconds, depending on the number of wavelengths being monitored. Effluent absorbances were converted to concentration and then both concentration and time were converted to normalized unitless parameters (C/C_0 and pore volumes respectively) to allow for comparison between different runs.

Retention characteristics of MSCKs were evaluated by extraction of MSCKs from the saturated porous media. This was accomplished by collected the saturated porous media from the column in 5 cm increments and washing each segment in an HCl solution (pH 3). The resulting supernatant was collected from each segment, neutralized using NaOH, and analyzed *via* UV-visible spectroscopy to determine the concentration of MSCK in each supernatant. The total volume of supernatant was then multiplied by the concentration to yield a total mass of MSCK retained in each 5-cm segment.

4.3.8. MSCK Sequestration Quantification

To determine the mass of mineral oil sequestered during FPS-1, the column effluent was monitored at 206 nm and at 212 nm. The resulting absorbance time series were then baseline corrected and resolved to solve the inequality:

$$A(206\,nm)_{Observed} = A(206\,nm)_{MSCK} + A(206\,nm)_{mineral\ oil}$$

$$A(212\,nm)_{Observed} = A(212\,nm)_{MSCK} + A(212\,nm)_{mineral\ oil}$$

$$A(206\,nm)_{MSCK} = \epsilon(206\,nm)_{MSCK} * b * C_{MSCK}$$

$$A(212\,nm)_{MSCK} = \epsilon(212\,nm)_{MSCK} * b * C_{MSCK}$$

$$A(206\,nm)_{MO} = \epsilon(206\,nm)_{MO} * b * C_{MO}$$

$$A(212\ nm)_{MO} = \epsilon(212\ nm)_{MO} * b * C_{MO}$$

in which the path length (b) is known (1 cm), each of the four molar absorptivity coefficients (ϵ) is known from the beer-lambert calibration curves, and $A(212\ nm)_{Observed}$ and $A(206\ nm)_{Observed}$ are measured absorbances at 212 nm and 206 nm respectively. This results in a system of 6 equations with 6 unknowns: $A(206\ nm)_{MSCK,}$ $A(206\ nm)_{MO}$, $A(212\ nm)_{MSCK),}$ $A(212\ nm)_{MO,}$ C_{MSCK} and C_{MO} which can then be solved to determine both C_{MSCK} and C_{MO}. With C_{MO} known, the total loading capacity of mineral oil in eluted MSCKs can be calculated using the following equation:

$$L = \frac{\int_{t_{10}}^{t_{90}} C_{MO} * \Delta t * Q}{0.8 * R_{MSCK} * V_{inj} * C_{inj}}$$

Where t_{90} and t_{10} are the 90% and 10% elution times for the MSCKs respectively, R_{MSCK} is the MSCK recovery, Δt is the time step between measurements (6 seconds), and V_{inj} and C_{inj} are the MSCK injection volume and concentration respectively.

This same process can be applied to the APS-1 and APS-2 to determine the concentration of MSCK in the effluent, however spectrophotometric methods are incapable of distinguishing between aqueous phase *m*-xylene and sequestered *m*-xylene.

For the quantification of *m*-xylene sequestration, aliquots were collected from the column effluent during the peak MSCK elution time of SC1 runs 2, 3, and 5. These aliquots were then centrifuged at 2500 rpm for 10 minutes using the Centricon Millipore's Ultracel-50. Ultracel centrifuge tubes consist of a retenate vial suspended over a sample reservoir. The retenate vial and sample reservoir are separated by a 100k molecular weight cut-off membrane, allowing *m*-xylene $_{(aq)}$ to pass to the sample

reservoir while retaining the MSCKs. In addition to the effluent samples, an aliquots of *m*-xylene contaminated water was collected from the feed reservoir and processed as the method baseline while an aliquot of μDIW was processed as the method blank. The samples were then analyzed via UV-vis to determine the concentration of *m*-xylene $_{(aq)}$ present in the column effluent

4.3.9. Mathematical Modeling

MSCK transport and retention was modeled using the advection dispersion equation modified with the addition of reversible and irreversible kinetic attachment terms:

$$\frac{\partial C}{\partial t} + \frac{\rho_b}{\theta_w}\left(\frac{\partial S_1}{\partial t} + \frac{\partial S_2}{\partial t}\right) = D_H \frac{\partial^2 C}{\partial x^2} + \frac{v_p \partial C}{\partial x}$$

where C is the concentration of MSCKs in solution, t is time, ρ_b is the bulk density of the solid phase, θ_w is the volumetric water content, S_1 is the concentration of MSCKs reversibly attached to the solid phase, S_2 is the concentration of the MSCKs irreversibly attached to the solid phase, D_H is the hydrodynamic dispersion coefficient, v_p is the pore water velocity, and x is the distance parallel to flow. The reversible and irreversible kinetic attachment processes can be expressed with the mass balance equations:

$$\frac{\rho_b}{\theta_w}\left(\frac{\partial S_1}{\partial t}\right) = C\ \psi_1\ k_{a1} - \frac{\rho_b}{\theta_w}\ k_{det}\ S$$

$$\frac{\rho_b}{\theta_w}\left(\frac{\partial S_2}{\partial t}\right) = C\ \psi_2\ k_{a2}$$

where k_{det} is the kinetic detachment rate for the reversible process while k_{a1} and k_{a2} are the kinetic attachment rates and ψ_1 and ψ_2 are the percent of the maximum MSCK

retention capacity (S_{max1} and S_{max2}) for the reversible and irreversible processes, respectively. S_{max1} and S_{max2} are related to the solid phase concentration as follows:

$$\psi_1 = \frac{S_{max1} - S_1}{S_{max1}}$$

$$\psi_2 = \frac{S_{max2} - S_2}{S_{max2}}$$

Note that for where S_{max1} and S_{max2} are much larger than S_1 and S_2, ψ_1 and ψ_2 approach unity.

Flow and transport of tracers and MSCKs were modeled using *pdpe*, a 1-D partial differential equation solver built into Matlab (see SI for example script). Parameter values were determined *via* inverse modeling using the *lsqnonlin* function, which implements the Levenberg-Marquardt Algorithm for nonlinear least-squares problems. This method is based on those described by Goldberg *et al.* in their comparison of ENP transport models [85].

4.4. Results

4.4.1. Conservative Tracer Test

For the sand only column (C1), the mean volumetric flow rate was 2.87 mL/s with a standard deviation (SD) of 0.07 mL/s and a standard error (SE) of 1.16% while the MRT for the conservative tracer was 22.58 min (0.14 SD, 2.80% SE) resulting in a calculated porosity of 0.503 (Table 6). The mean recovery of the Br^- tracer was 96% (0.051 SD, 0.023 SE).

For the sand column with free phase mineral oil (C2), the Br^- tracer tests yielded a residence time of 12.87 min with a standard deviation of 0.65 min and a standard error

Table 6 – Br^- conservative tracer test results

Column	Residence Time [min]			Volumetric Flow Rate [mL/s]		
	Mean	Standard Deviation	Standard Error	Mean	Standard Deviation	Standard Error
C1	22.58	0.14	2.80%	2.87	0.074	0.033
C2	12.87	0.65	2.53%	5.31	0.029	0.014
C3	11.20	0.12	0.40%	4.90	0.033	0.015

of 2.5% (Table 6). These values yielded a calculated porosity of 0.532. Accounting for the 200 ml of NAPL, this brings the total porosity to 0.5576, which is much higher than the porosity for column C1. This increase in porosity is likely due to difficulties inherent in the packing process caused by the presence of mineral oil. The inclusion of air bubbles within the mineral oil was also problematic and the buoyant force of the mineral oil may have contributed to the poor degree of compaction. The mean recovery of the Br^- tracer was 92% (0.007 SD, 0.003 SE).

For the sand/clay column (C3), a recovery of 99.86% (0.005 SD, 0.002 SE) was achieved with a mean residence time of 11.2 minutes (0.12 min SD, 0.40% SE) (Table 6), yielding a calculated porosity of 0.426.

4.4.2. MSCK Transport

The results of Trans-1 (Figure 8b) indicate that MSCKs were able to transport readily through column C1, with a 99% recovery. The MRT of the MSCKs was 0.966 pore volumes compared to the calculated 1.06 pore volume MRT of the conservative tracer in C1 (Figure 8a). The shift in MRT was shown to be significant in a two tail t-test. Because the MSCK were behaving as conservative, effective porosity for the

MSCKs was calculated following the same methods described for the Br^- tracer test, yielding an effective porosity of 0.481

Trans-2 (Figure 8e) yielded only a 63% recovery (0.009 SD, 0.004 SE), but reported a residence time of 0.960 pore volumes (SD 0.010, 0.005 SE) which was shown to be insignificant relative to Trans-1 in a two tail t-test (Table 7).

The presence of *m*-xylene$_{(aq)}$ in APS-1 (Figure 8c) exhibited no significant difference in residence time relative to Trans-1, however, recovery of MSCKs was reduced from 99% to 61% (Table 7). In contrast, the presence of free phase mineral oil in FPS-1 (Figure 8h) retarded the transport of MSCKs, reducing the MRT to 1.010 pore volumes (Table 7). The presence of NAPL also had an interesting effect of the repeatability of MSCK recovery. Although error in the MRT of the MSCKs was negligible, recovery varied drastically, ranging from 44% to 82% with a mean of 66% and a SD of 17.5 pp.

The variability of MSCK recovery was much higher in FPS-1 than in any other treatment, with recovery increasing after each application and ranging from 43% to 83% with a mean of 65.85% and a standard deviation of 0.1751 (Table 7). The standard error was also the largest of any other test at 0.0875. Conversely, residence time had the inverse trend, decreasing after each application from 1.04 pore volumes in the first injection to 0.980 in the fourth. Coincidently, the fifth treatment was uncharacteristic of all four of the other treatments, increasing in residence time to 1.28 pore volumes, but also displaying the highest elution of mineral oil, as such this treatment was treated as an outlier.

The presence of clays and *m*-xylene $_{(aq)}$ in APS-2 resulted in the highest retardation of any experiment, with a MSCK residence time of 1.039 pore volumes (Table 7).

Table 7 – Transport characteristics of MSCKs			**None**	***m*-Xylene$_{(aq)}$**	**Mineral oil**
Residence Time	Sand	$\bar{x}$ [pore volumes]	0.9660	0.9660	1.01
		σ [pore volumes]	0.0267	0.0012	0.027
		SE [%]	1.234	0.050	1.359
	Sand/Clay	$\bar{x}$ [pore volumes]	0.960	1.039	-
		σ [pore volumes]	0.010	0.016	-
		SE [%]	0.489	0.710	-
Recovery	Sand	$\bar{x}$ [%]	99	61	67
		σ [pp]	3.5	7.4	17.5
		SE [pp]	1.2	3.0	8.8
	Sand/Clay	$\bar{x}$ [%]	63	53	-
		σ [pp]	0.9	5.0	-
		SE [pp]	0.4	2.3	-

Mean ($\bar{x}$), standard deviation (σ), and standard error (SE) for residence time and recovery in sand and sand/clay column experiments

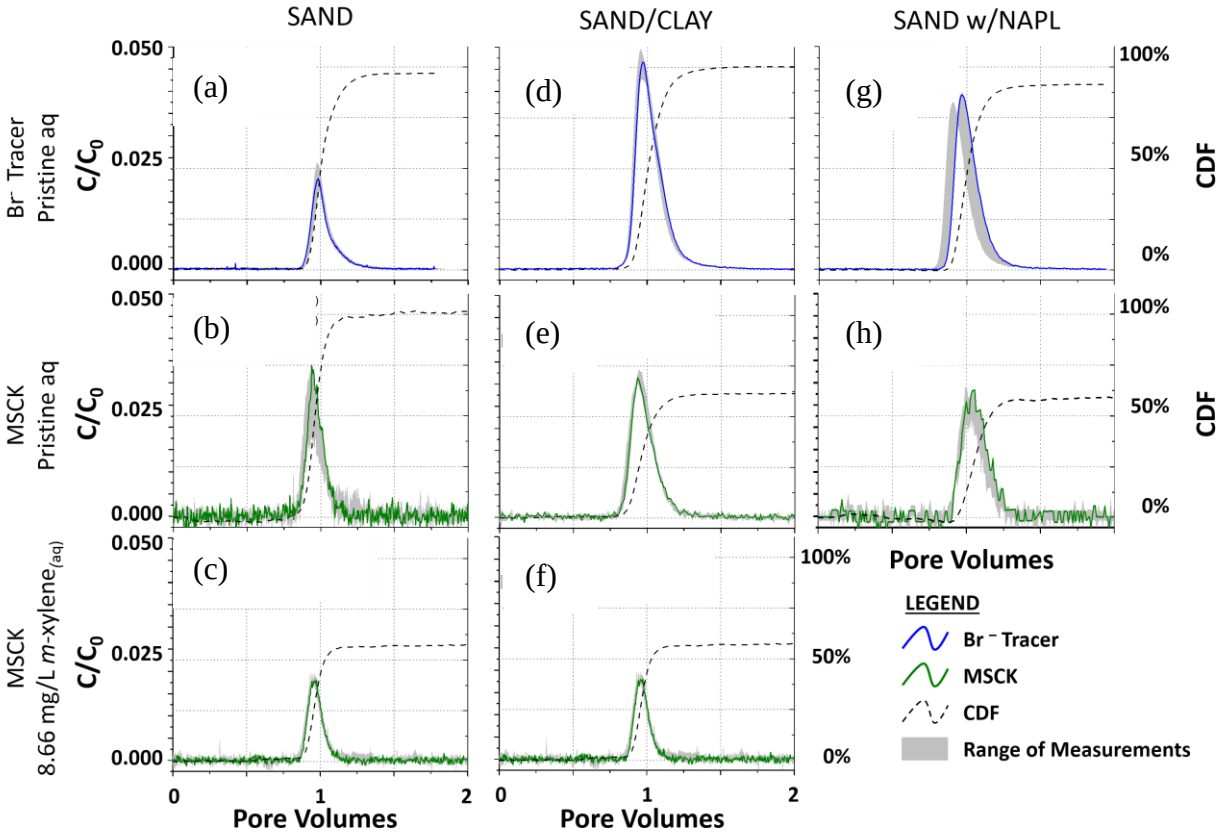

Figure 8 - Representative breakthrough curves and cumulative distribution functions for each experiment. The range of all experimental values is depicted in the shaded grey area. (a) Br^- tracer in sand column (b) MSCK in sand column (c) MSCK in sand column with *m*-xylene contaminated aq phase (d) Br^- tracer in sand/clay column € MSCK in sand/clay column (f) MSCK in sand/clay column with *m*-xylene contaminated aqueous phase (g) Br^- tracer in sand column with NAPL (h) MSCK in sand column with NAPL.

4.4.3. Contaminant Sequestration

The mineral oil BTCs generated by the resolution of A_{MO} and A_{MSCK} exhibit low signal to noise ratios, with peak absorbances for mineral within an order of magnitude of measurement noise. Because of the low signal to noise ratio, there is limited confidence in the reproducibility and the precision of the mineral oil sequestration calculations and

as such all values are considered approximate and are reduced to a single significant figure, ranging from Mineral oil sequestration was calculated to a loading capacity of between 0.1 and 0.03 mg of mineral oil per mg of MSCK eluted.

Aqueous phase *m*-xylene in APT2 was non-detect in the column effluent during MSCK elution. The BTC for *m*-xylene $_{(aq)}$ in APS-1 and APS-2 exhibited low signal to noise ratios, but also low variability and as such, average *m*-xylene and MSCK BTC were able to be generated using the signal stacking method. The resulting average BTCs for MSCKs were was statistically members of the populations of the individual BTCs indicating that signal stacking for the generation of BTC was valid. The average *m*-xylene BTC reveals a spike in *m*-xylene concentration in post 1.00 pore volumes with a trough pre 1.00 pore volumes wake of the MSCKs (Figure 9).

4.5. Discussion

4.5.1. Transport and Deposition

The 99% recovery of Trans-1 indicate that MSCKs transport readily through saturated sand with no losses caused by irreversible attachment or pore throat clogging. The shift in residence time between the MSCKs in Trans-1 and the C1 Br^- tracer in conjuncture with the lack of change in distribution suggests that some pore size exclusion occurs during transport. This shift also implies that MSCKs transmit through sand faster than soluble species, allowing for MSCKs to overtake soluble species wave fronts *in situ*. Because of the conservative behavior MSCKs, the effective porosity of C1was able to be calculated (0.481) and compared to the porosity calculated for C1 using the Br^- tracer (0.503). This difference is indicative that roughly 4.4% of the pore

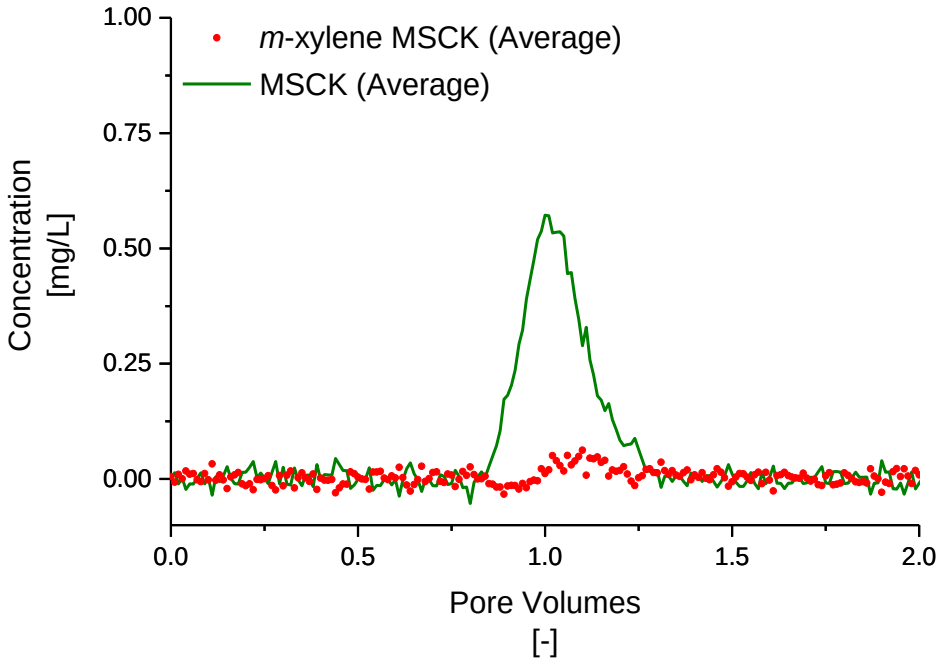

Figure 9 - Fluctuations in concentration of *m*-xylene$_{(aq)}$ above the baseline caused by differences in the pore water velocity of *m*-xylene$_{(aq)}$ and MSCKs.

spaces are inaccessible to MSCKs during Trans-1. Given the relative size of the MSCKs (72 nm) to the sand particles (207 μm), this size exclusion is either indicative of pore size exclusion which would indicate homoaggregation of MSCKs or is a function of the particle velocity/inertia. Further testing over a range of fluid and particle velocities is needed to determine the contributions of both of these two factors to the shift in residence time.

The inclusion of clay particles in the saturated porous provides the MSCKs with sorption surfaces as well as charged surfaces in which van der Waals interactions can

take place, potentially leading to kinetic attachment or heteroaggregation of MSCKs and clay particles. Additionally, the clay particles are significantly smaller than the sand and lead to a decrease in porosity and a decrease in pore throat sizes. The residence time of Trans-2 was insignificantly different that the residence time of Trans-1, indicating that the smaller pore sizes associated with the inclusion of clays did not affect transport of MSCKs. The reduction in recovery from 99% to 63%, however, is indicative of either irreversible attachment of MSCKs to clay particles or pore throat straining of MSCK aggregates.

Adding the presence of aqueous phase contaminants to C1 did not affect the residence time, however, recovery was reduced from 99% in Trans-1 to 61% in APS-1. In contrast, the presence of *m*-xylene $_{(aq)}$ in a sand/clay environment not only reduced the recovery from 63% to 53%, but also increased the residence time of the MSCKs from 0.96 pore volumes in Trans-2 to 1.04 pore volumes in APS-2. Given that the *m*-xylene $_{(aq)}$ has no effect on the residence time of MSCKs in sand and given that the difference in the MSCK residence times in sand and sand/clay columns in the absence of *m*-xylene $_{(aq)}$ is insignificant, the shift in residence time in APS-2 is indicative that the clay has additional modes of retardation in the presence of *m*-xylene $_{(aq)}$. One possibility is that the increase in residence time is due to reversible attachment/detachment of MSCKs caused by competition between sequestration of *m*-xylene by the MSCKs and sorption of *m*-xylene by the clay.

The presence of free phase mineral oil in sand (FPS-1) caused great variability in MSCK recovery of all treatment, with an apparent time dependent increase in recovery.

Recovery increased after each treatment ranging from 44% in treatment 1 to 82% in treatment 4. Treatment 5 was uncharacteristic of all other treatments and was excluded as an outlier.

4.5.2. Contaminant Sequestration

Variability in FPS-1 limits the confidence in the mineral oil sequestration calculation of the MSCKs; however, the MSCKs performed well below the maximum loading capacity of 10 mg mineral oil per mg of MSCK. This may be because only eluted MSCKs were considered and that loaded MSCKs are retained. The results of the transport experiment support the hypothesis that particle aggregation is more likely to occur in the presence of hydrophobic species. It is possible that the low observed mineral oil recovery is partially due to loaded MSCKs aggregating and being unable to elute from the column,

The sequestration of aqueous phase *m*-xylene was nearly 100% of the aqueous phase *m*-xylene. Sequestration of aqueous phase *m*-xylene during transport was verified in *m*-xylene BTC in which a negative and positive peak are visible in *m*-xylene concentration (Figure 9). Although the spectrophotometer is unable to differentiate between aqueous phase and sequestered *m*-xylene, the positive and negative peaks are caused by difference in particle and pore water velocity. As contaminated waters mix with the MSCK slug during transport, MSCKs near the rear of the injection slug are allowed to sequester *m*-xylene $_{(aq)}$ before it comes in contact with the rest of the slug, thereby lowering the aqueous phase *m*-xylene concentration below ambient concentration. Because of this, MSCKs at the front of the injection slug are continually

exposed to an aqueous phase with an *m*-xylene concentration below the ambient 8.66 mg/L baseline concentration. As a result, particles which are eluted earlier are exposed to less *m*-xylene$_{(aq)}$ and exist within a packet of water which was treated as it passed through the rear of the MSCK injection slug, causing the detected *m*-xylene concentration to be below the ambient (aka baseline) concentration. Conversely, MSCKs which are eluted later are exposed to a continually refreshing source of ambient aqueous phase *m*-xylene and are therefore able to sequester more than 8.66 mg/L of *m*-xylene, resulting in a rise of the *m*-xylene BTC above the baseline.

4.6. Conclusions

This study determined that MSCKs are transported readily through saturated sands with virtually no particle retention; however, the presence of clays retards MSCK transport *via* irreversible attachment and/or aggregation and straining of MSCKs. Additionally, the presence of hydrocarbon contaminants, in either the aqueous phase or as free phase, reduces the mobility of MSCKs and lowers recovery.

The findings of the sequestration experiments indicate that MSCKs are excellent at treating aqueous phase contaminants during transport, with *m*-xylene$_{(aq)}$ being removed below the detection limit and well below the regulatory limits for residential groundwater. The sequestration of free phase mineral oil by MSCKs was significantly lower, with mineral oil recovery totaling only between 3% and 10% of the total mass of MSCKs injected.

The change in transport properties of MSCKs in the presence of aqueous phase contaminants has a number of potential applications: One possibility is the encapsulation

or immobilization of existing contaminant plumes. Also, it should be noted that NAPL contaminants in nature tend to equilibrate with surrounding aqueous phase and create local regions of high aqueous phase concentrations in the vicinity of the NAPL. There is potential to make use of these properties to create treatment zones around NAPL contamination, essentially creating small scale permeable reactive barriers around the free phase liquid.

5. SUMMARY

This project has studied the transport characteristics and remediation capabilities of MSCKs in saturated porous media. Transport characteristics were determined by conducting one dimensional impulse column experiments in saturated sand and saturated sand/clay columns.

This study determined that, although some pore size exclusion does occur, MSCKs are readily transported through saturated sand, with 99% recovery observed. In sand/clay, irreversible attachment, aggregation, and/or straining of MSCKs occurs, reducing recovery to 63%. The presence of aqueous phase and free phase contaminants was also found to retard MSCK transport. In the presence of ambient 8.66 mg/L *m*-xylene $_{(aq)}$, MSCK recovery was reduced to 61% in sand and 53% in sand/clay. Additionally, the presence of aqueous phase *m*-xylene exhibited increase in MSCK residence time from 0.966 pore volumes to 1.04 pore volumes. The presence of free phase mineral oil had similar effects, with recovery being reduced to 66% and residence time increasing to 1.01 pore volumes.

The sequestration of contaminants during transport was also studied with aqueous phase *m*-xylene during MSCK elution being reduced to below the method detection limit. The sequestration of free phase contaminant performed much worse, with the mass of mineral oil recovery being between 10% and 3% of the mass of MSCKs eluted.

In conclusion, MSCKs are a viable groundwater remediation technology for aqueous phase contaminants, however they exhibit difficulties in the sequestration of

free phase contaminants. The effect that the presence of contaminants have on the transport characteristics of MSCKs could potentially be beneficial for the entrapment or immobilization of contaminant plumes, however additional work is needed to explore this possibility.

Although this body of work has advanced the understanding of MSCK transport in saturated porous media, more work is still needed to fully characterize their transport characteristics. The effects of flow rate, presence of salts, changes in pH, and particle aggregation on MSCK transport and sequestration have not yet been determined and the existing experimental data has not yet been successfully fit to a numerical model. Furthermore, retention profiles for the MSCKs within the soil matrix have not yet been produced and are necessary for the calibration of any numerical model.

REFERENCES

1. Zhang, W. X., Nanoscale iron particles for environmental remediation: An overview. *Journal of Nanoparticle Research* **2003,** *5*, (3-4), 323-332.

2. Qu, X.; Alvarez, P. J. J.; Li, Q., Applications of nanotechnology in water and wastewater treatment. *Water Research* **2013,** *47*, (12), 3931-3946.

3. International Organization for Standardization, ISO/TC 229: Nanotechnologies, *ISO TS 80004-1:2010 – Nanotechnologies – Vocabulary Part 1 – Core terms*. Geneva, Switzerland, 2010.

4. Auffan, M.; Rose, J.; Bottero, J.-Y.; Lowry, G. V.; Jolivet, J.-P.; Wiesner, M. R., Towards a definition of inorganic nanoparticles from an environmental, health and safety perspective. *Nature Nanotechnology* **2009,** *4*, (10), 634-641.

5. Buzea, C.; Blandino, I. I. P.; Robbie, K., Nanomaterials and nanoparticles: Sources and toxicity. *Biointerphases* **2007,** *2*, (4), MR17 - MR172.

6. Zhang, W.-x.; Elliott, D. W., Applications of iron nanoparticles for groundwater remediation. *Remediation Journal* **2006,** *16*, (2), 7-21.

7. Tratnyek, P. G.; Johnson, R. L., Nanotechnologies for environmental cleanup. *Nano Today* **2006,** *1*, (2), 44-48.

8. Wilson, R. F., Nanotechnology: the challenge of regulating known unknowns. *Journal of Law, Medicine & Ethics* **2006,** *Winter*, 704-713.

9. Tsuji, J. S.; Maynard, A. D.; Howard, P. C.; James, J. T.; Lam, C. W.; Warheit, D. B.; Santamaria, A. B., Research strategies for safety evaluation of nanomaterials, part IV: risk assessment of nanoparticles. *Toxicological sciences : an official journal of the Society of Toxicology* **2006,** *89*, (1), 42-50.

10. Fortner, J. D.; Lyon, D. Y.; Sayes, C. M.; Boyd, A. M.; Falkner, J. C.; Hotze, E. M.; Alemany, L. B.; Tao, Y. J.; Guo, W.; Ausman, K. D.; Colvin, V. L.; Hughes, J. B.,

C60 in water: nanocrystal formation and microbial response. *Environmental Science & Technology* **2005,** *39*, (11), 4307-4316.

11. Lyon, D. Y.; Adams, L. K.; Falkner, J. C.; Alvarez, P. J. J., Antibacterial Activity of Fullerene Water Suspensions: Effects of Preparation Method and Particle Size†. *Environmental Science & Technology* **2006,** *40*, (14), 4360-4366.

12. Adams, L. K.; Lyon, D. Y.; Alvarez, P. J. J., Comparative eco-toxicity of nanoscale TiO2, SiO2, and ZnO water suspensions. *Water Research* **2006,** *40*, (19), 3527-3532.

13. He, F.; Zhao, D., Preparation and characterization of a new class of starch-stabilized bimetallic nanoparticles for degradation of chlorinated hydrocarbons in water. *Environmental Science & Technology* **2005,** *39*, (9), 3314-20.

14. Mondal, K.; Jegadeesan, G.; Lalvani, S. B., Removal of selenate by Fe and NiFe nanosized particles. *Industrial & Engineering Chemistry Research* **2004,** *43*, (16), 4922-4934.

15. Schrick, B.; Hydutsky, B. W.; Blough, J. L.; Mallouk, T. E., Delivery vehicles for zerovalent metal nanoparticles in soil and groundwater. *Chemistry of Materials* **2004,** *16*, (11), 2187-2193.

16. Brant, J. A.; Labille, J.; Robichaud, C. O.; Wiesner, M., Fullerol cluster formation in aqueous solutions: Implications for environmental release. *Journal of Colloid and Interface Science* **2007,** *314*, (1), 281-288.

17. Pelley, A. J.; Tufenkji, N., Effect of particle size and natural organic matter on the migration of nano- and microscale latex particles in saturated porous media. *Journal of Colloid and Interface Science* **2008,** *321*, (1), 74-83.

18. Pavía-Sanders, A.; Zhang, S.; Flores, J. A.; Sanders, J. E.; Raymond, J. E.; Wooley, K. L., Robust magnetic/polymer hybrid nanoparticles designed for crude oil entrapment and recovery in aqueous environments. *ACS Nano* **2013,** *7*, (9), 7552-7561.

19. USEPA *Cleaning Up the Nation's Waste Sites: Markets and Technology Trends*; United States Environmental Protection Agency: September 2004, 2004.

20. USEPA *Semiannual Report Of UST Performance Measures End Of Fiscal Year 2014 (October 1, 2013 – September 30, 2014)*; http://www.epa.gov/swerust1/cat/ca-14-34.pdf, November 2014, 2014; p 12.

21. USEPA *Superfund Remedy Report*; EPA 542-R-13-016; USEPA: November 2013, 2013.

22. Khan, F. I.; Husain, T.; Hejazi, R., An overview and analysis of site remediation technologies. *Journal of Environmental Management* **2004,** *71*, 95-122.

23. Siegrist, R. L.; Crimi, M.; Simpkin, T. J., *In Situ Chemical Oxidation for Groundwater Remediation*. Springer New York: 2011.

24. Waldemer, R. H.; Tratnyek, P. G.; Johnson, R. L.; Nurmi, J. T., Oxidation of chlorinated ethenes by heat-activated persulfate: kinetics and products. *Environmental Science & Technology* **2007,** *41*, (3), 1010-1015.

25. Jacobs, J. A., Fenton's reaction and groundwater remediation. In *Water Encyclopedia*, John Wiley & Sons, Inc.: 2005.

26. USEPA *In Situ and Ex Situ Biodegradation Technologies for Remediation of Contaminated Sites*; United States Environmental Protection Agency: October 2006, 2006.

27. Jacobs, J. A.; Testa, S. M., Design considerations for in situ chemical oxidation using high pressure jetting technology. *AEHS Contaminated Soil Sediment & Water* **2003,** *2003*, (March/April), 51-59.

28. Watts, R. J.; Haeri-McCarroll, T. M.; Teel, A. L., Effect of contaminant hydrophobicity in the treatment of contaminated soils by catalyzed H2O2 propagations (modified Fenton's reagent). *Journal of Advanced Oxidation Technologies* **2008,** *11*, (2), 354-361.

29. Lundstedt, S.; Persson, Y.; Oberg, L., Transformation of PAHs during ethanol-Fenton treatment of an aged gasworks' soil. *Chemosphere* **2006,** *65*, (8), 1288-1294.

30. Bogan, B.; Trbovic, V., Effect of sequestration on PAH degradability with Fenton's reagent: roles of total organic carbon, humin, and soil porosity. *Journal of Hazardous Materials* **2003,** *100*, (1-3), 285-300.

31. Dugan, P. J. Coupling surfactants/cosolvents with oxidants: Effects on remediation and performance assessment. Dissertation, Colorado School of Mines, 2008.

32. Boopathy, R., Factors limiting bioremediation technologies. *Bioresource Technology* **2000,** *74*, (1), 63-67.

33. Pollard, S. J. T.; Hrudey, S. E.; Fedorak, P. M., Bioremediation of petroleum- and creosote-contaminated soils: a review of constraints. *Waste Management & Research* **1994,** *12*, (2), 173-194.

34. Rayu, S.; Karpouzas, D.; Singh, B., Emerging technologies in bioremediation: constraints and opportunities. *Biodegradation* **2012,** *23*, (6), 917-926.

35. Speight, J.; Arjoon, K., *Bioremediation of Petroleum and Petroleum Products*. Scrivener Publishing LLC: 2012.

36. Albergaria, J. T.; Alvim-Ferraz, M. d. C. M.; Delerue-Matos, C., Remediation of sandy soils contaminated with hydrocarbons and halogenated hydrocarbons by soil vapour extraction. *Journal of Environmental Management* **2012,** *104*, (0), 195-201.

37. Zhao, L.; Zytner, R. G., Estimation of SVE closure time. *Journal of Hazardous Materials* **2008,** *153*, (1–2), 575-581.

38. Scherer, M. M.; Richter, S.; Valentine, R. L.; Alvarez, P. J. J., Chemistry and microbiology of permeable reactive barriers for in situ groundwater clean up. *Critical Reviews in Microbiology* **2000,** *26*, (4), 221-264.

39. Council), I. I. T. R. *Permeable reactive barrier: technology update*; Interstate Technology & Regulatory Council, PRB: Technology Update Team.: Washington D.C., June 2011, 2011.

40. Thiruvenkatachari, R.; Vigneswaran, S.; Naidu, R., Permeable reactive barrier for groundwater remediation. *Journal of Industrial and Engineering Chemistry* **2008,** *14*, (2), 145-156.

41. Roehl, K. E.; Meggyes, T.; Simon, F. G.; Stewart, D. I., *Long-Term Performance of Permeable Reactive Barriers*. Elsevier Science: 2005.

42. Bezbaruah, A. N.; Krajangpan, S.; Chisholm, B. J.; Khan, E.; Elorza Bermudez, J. J., Entrapment of iron nanoparticles in calcium alginate beads for groundwater remediation applications. *Journal of Hazardous Materials* **2009,** *166*, (2–3), 1339-1343.

43. Chang, M. C.; Shu, H. Y.; Hsieh, W. P.; Wang, M. C., Using nanoscale zero-valent iron for the remediation of polycyclic aromatic hydrocarbons contaminated soil. *Journal of the Air & Waste Management Association* **2005,** *55*, (8), 1200-7.

44. Ponder, S. M.; Darab, J. G.; Mallouk, T. E., Remediation of Cr(VI) and Pb(II) aqueous solutions using supported, nanoscale zero-valent iron. *Environmental Science & Technology* **2000,** *34*, (12), 2564-2569.

45. Krajangpan, S.; Kalita, H.; Chisholm, B. J.; Bezbaruah, A. N., Iron nanoparticles coated with amphiphilic polysiloxane graft copolymers: dispersibility and contaminant treatability. *Environmental Science & Technology* **2012,** *46*, (18), 10130-10136.

46. Krol, M. M.; Oleniuk, A. J.; Kocur, C. M.; Sleep, B. E.; Bennett, P.; Xiong, Z.; O'Carroll, D. M., A field-validated model for in situ transport of polymer-stabilized nZVI and implications for subsurface injection. *Environmental Science & Technology* **2013,** *47*, (13), 7332-7340.

47. Phenrat, T.; Cihan, A.; Kim, H.-J.; Mital, M.; Illangasekare, T.; Lowry, G. V., Transport and deposition of polymer-modified Fe0 nanoparticles in 2-D heterogeneous porous media: effects of particle concentration, Fe0 content, and coatings. *Environmental Science & Technology* **2010,** *44*, (23), 9086-9093.

48. Kanel, S. R.; Choi, H., Transport characteristics of surface-modified nanoscale zero-valent iron in porous media. *Water Science And Technology* **2007,** *55*, (1-2), 157-162.

49. Mauter, M. S.; Elimelech, M., Environmental applications of carbon-based nanomaterials. *Environmental Science & Technology* **2008,** *42*, (16), 5843-59.

50. Yang, K.; Zhu, L.; Xing, B., Adsorption of polycyclic aromatic hydrocarbons by carbon nanomaterials. *Environmental Science & Technology* **2006,** *40*, (6), 1855-61.

51. Li, Y.-H.; Li, S.; Wang, Z.; Luan, J.; Ding, C.; Xu, D., Adsorption of cadmium(II) from aqueous solution by surface oxidized carbon nanotubes. *Carbon* **2003,** *41*, (5), 1057-1062.

52. Limbach, L. K.; Wick, P.; Manser, P.; Grass, R. N.; Bruinink, A.; Stark, W. J., Exposure of engineered nanoparticles to human lung epithelial cells: influence of chemical composition and catalytic activity on oxidative stress. *Environmental Science & Technology* **2007,** *41*, (11), 4158-63.

53. Azevedo Costa, C. L.; Chaves, I. S.; Ventura-Lima, J.; Ferreira, J. L. R.; Ferraz, L.; de Carvalho, L. M.; Monserrat, J. M., In vitro evaluation of co-exposure of arsenium and an organic nanomaterial (fullerene, C60) in zebrafish hepatocytes. *Comparative Biochemistry and Physiology Part C: Toxicology & Pharmacology* **2012,** *155*, (2), 206-212.

54. Baun, A.; Hartmann, N. B.; Grieger, K.; Kusk, K. O., Ecotoxicity of engineered nanoparticles to aquatic invertebrates: a brief review and recommendations for future toxicity testing. *Ecotoxicology* **2008,** *17*, (5), 387-95.

55. Bauna, A.; Sørensena, S. N.; Rasmussena, R. F.; Hartmanna, N. B.; Kochb, C. B., Toxicity and bioaccumulation of xenobiotic organic compounds in the presence of aqueous suspensions of aggregates of nano-C 60. *Aquatic Toxicology* **2008,** *86*, (3), 379-387.

56. Sun, H.; Zhang, X.; Zhang, Z.; Chen, Y.; Crittenden, J. C., Influence of titanium dioxide nanoparticles on speciation and bioavailability of arsenite. *Environmental Pollution* **2009,** *157*, (4), 1165-1170.

57. Tungittiplakorn, W.; Lion, L. W.; Cohen, C.; Kim, J.-Y., Engineered polymeric nanoparticles for soil remediation. *Environmental Science & Technology* **2004,** *38*, (5), 1605-1610.

58. Bystrzejewska-Piotrowska, G.; Golimowski, J.; Urban, P. L., Nanoparticles: their potential toxicity, waste and environmental management. *Waste Management & Research* **2009,** *29*, (9), 2587-95.

59. Hankina, S.; Boraschib, D.; Duschlc, A.; Lehrd, C.-M.; Lichtenbelde, H., Towards nanotechnology regulation – Publish the unpublishable. *Nanotoday* **2011,** *6*, (3), 228-231.

60. Council, N. S. a. T., National Nanotechnology Initiative Environmental, Health, and Safety Research Strategy. In Subcommittee on Nanoscale Science, E., and Technology, Ed. National Nanotechnology Initiative: 2011.

61. Thomas, K.; Sayre, P., Research strategies for safety evaluation of nanomaterials, Part I: evaluating the human health implications of exposure to nanoscale materials. *Toxicological sciences : an official journal of the Society of Toxicology* **2005,** *87*, (2), 316-21.

62. USEPA Control of Nanoscale Materials under the Toxic Substances Control Act. http://www.epa.gov/oppt/nano/ (May 7, 2013),

63. USEPA Office of Research and Development. Final Nanomaterial Research Strategy (NRS). http://www.epa.gov/ord/index.htm

64. Kalambur, V. S.; Han, B.; Kim, B.-S.; Taton, T. A.; Bischof, J. C., In vitro characterization of movement, heating and visualization of magnetic nanoparticles for biomedical applications. *Nanotechnology* **2005,** *16*, (8), 1221-1233.

65. Wang, C.; Bobba, A. D.; Attinti, R.; Shen, C.; Lazouskaya, V.; Wang, L.-P.; Jin, Y., Retention and transport of silica nanoparticles in saturated porous media: effect of concentration and particle size. *Environmental Science & Technology* **2012,** *46*, (13), 7151-8.

66. Lecoanet, H. F.; Wiesner, M. R.; Bottero, J.-Y., Laboratory assessment of the mobility of nanomaterials in porous media. *Environmental Science & Technology* **2004,** *38*, (19), 5164-9.

67. Ben-Moshe, T.; Dror, I.; Berkowitz, B., Transport of metal oxide nanoparticles in saturated porous media. *Chemosphere* **2010,** *81*, (3), 387-393.

68. Lecoanet, H. F.; Wiesner, M. R., Velocity effects on fullerene and oxide nanoparticle deposition in porous media. *Environmental Science & Technology* **2004,** *38*, (16), 4377-82.

69. Jaisi, D. P.; Saleh, N. B.; Blake, R. E.; Elimelech, M., Transport of single-walled carbon nanotubes in porous media: filtration mechanisms and reversibility. *Environmental Science & Technology* **2008,** *42*, (22), 8317-23.

70. Li, Z.; Li, E.; Sahle Demessie, A.; Hassan, G., Transport and deposition of CeO2 nanoparticles in water-saturated porous media. *Water Research* **2011,** *45*, (15), 4409-4418.

71. Seymour, M. Transport of Engineered Nanomaterials in Porous Media: Groundwater Remediation Application and Effects of Particle Shape. University of Nebraska-Lincoln, Lincoln, Nebraska, 2012.

72. Darlington, T.; Darlington, A.; Neigh, M.; Spencer, O.; Nguyen, S., Nano particle characteristics affecting environmental fate and transport through soil. *Environmental Toxicology and Chemistry* **2009,** *28*, (6), 1191-9.

73. Chowdhury, I.; Chowdhury, Y.; Hong, R.; Honda, S., Mechanisms of TiO2 nanoparticle transport in porous media: Role of solution chemistry, nanoparticle concentration, and flowrate. *Journal of Colloid and Interface Science* **2011,** *360*, (2), 548-555.

74. Godinez, I. G.; Darnault, C. J. G., Aggregation and transport of nano-TiO2 in saturated porous media: Effects of pH, surfactants and flow velocity. *Water Research* **2011,** *45*, (2), 839-851.

75. Guzman, K. A. D.; Finnegan, M. P.; Bandield, J. F., Influence of surface potential on aggregation and transport of titania nanoparticles. *Environmental Science & Technology* **2006,** *40*, (24), 7688-93.

76. Aiken, G.; Aiken, H.; Hsu Kim, J., Influence of dissolved organic matter on the environmental fate of metals, nanoparticles, and colloids. *Environmental Science & Technology* **2011,** *45*, (8), 3196-3201.

77. Tufenkji, N.; Elimelech, M., Spatial distributions of cryptosporidium oocysts in porous media: evidence for dual mode deposition. *Environmental Science & Technology* **2005,** *39*, (10), 3620-9.

78. Johnson, P. R.; Elimelech, M., Dynamics of colloid deposition in porous media: blocking based on random sequential adsorption. *Langmuir* **1995,** *11*, (3), 801-812.

79. Schijven, J. F.; Hassanizadeh, S. M.; de Bruin, R. H. A. M., Two-site kinetic modeling of bacteriophages transport through columns of saturated dune sand. *Journal of Contaminant Hydrology* **2002,** *57*, (3), 259-279.

80. Yao, K.-m.; Habibian, M. T.; O'Melia, C. R., Water and waste water filtration. Concepts and applications. *Environmental Science & Technology* **1971,** *5*, (11), 1105-1112.

81. Foppena, J. W.; Herwerdena, M. v.; Schijvenb, J., Transport of Escherichia coli in saturated porous media: Dual mode deposition and intra-population heterogeneity. *Water Research* **2007,** *41*, (8), 1743-1753.

82. Simunek, J.; He, C.; Pang, L.; Bradford, S. A., Colloid-facilitated solute transport in variably saturated porous media: numerical model and experimental verification. *Vadose zone journal* **2006,** *5*, (3), 1035-1047.

83. Li, Y.; Wang, Y.; Pennell, K. D.; Abriola, L. M., Investigation of the transport and deposition of fullerene (C60) nanoparticles in quartz sands under varying flow conditions. *Environmental Science & Technology* **2008,** *42*, (19), 7174-80.

84. Derjaguin, B.; Landau, L., Theory of the stability of strongly charged lyophobic sols and of the adhesion of strongly charged particles in solutions of electrolytes. *Progress in Surface Science* **1993,** *43*, (1), 30-59.

85. Goldberg, E.; Scheringer, M.; Bucheli, T. D.; Hungerbühler, K., Critical assessment of models for transport of engineered nanoparticles in saturated porous media. *Environmental Science & Technology* **2014,** *48*, (21), 12732-12741.

86. Petosa, A. R.; Jaisi, D. P.; Quevedo, I. R.; Elimelech, M.; Tufenkji, N., Aggregation and deposition of engineered nanomaterials in aquatic environments: role of physicochemical interactions. *Environmental Science & Technology* **2010,** *44*, (17), 6532-49.

87. Cornelis, G.; Pang, L.; Doolette, C.; Kirby, J. K.; McLaughlin, M. J., Transport of silver nanoparticles in saturated columns of natural soil. *Science of the Total Environment* **2013,** *463-464*, 120-130.

88. Texas Gold 40/70 raw sand, Fact Sheet. In *FTSI International*, FTSI International: 2008.

89. Murray, H. H., *Applied Clay Mineralogy Occurrences, Processing and Application of Kaolins, Bentonites, Palygorskite-Sepiolite, and Common Clays*. 1st ed.; 2006; Vol. 2.

90. Conley, R. F. In *Statistical distribution patterns of particle size and shape in the Georgia kaolins*, Fourteenth National Conference on Clays and Clay Minerals, Berkeley, Ca, 1966; Pergamon Press: Berkeley, Ca, 1966.

91. Sanemasa, I.; Araki, M.; Deguchi, T.; Nagai, H., Solubility measurements of benzene and the alkylbenzenes in water by making use of solute vapor. *Bulletin of the Chemical Society of Japan* **1982,** *55*, (4), 1054-1062.

92. TCEQ, TRRP Protective Concentration Levels. In Texas Commission on Environmental Quality: 2014.

93. Standard test method for permeability of granular soils (constant head). In *ASTM Standard D2434-68*, ASTM International: West Conshohocken, PA, 2006.

94. Karn, B.; Kuiken, T.; Otto, M., Nanotechnology and in situ remediation: a review of the benefits and potential risks. *Environmental Health Perspectives* **2009,** *117*, (12), 1823-1831.

95. Musee, N., Nanowastes and the environment: potential new waste management paradigm. *Environment international* **2011,** *37*, (1), 112-28.

96. Calcagnile, P.; Fragouli, D.; Bayer, I. S.; Anyfantis, G. C.; Martiradonna, L.; Cozzoli, P. D.; Cingolani, R.; Athanassiou, A., Magnetically driven floating foams for the removal of oil contaminants from water. *ACS Nano* **2012,** *6*, (6), 5413-5419.

97. Cong, H.-P.; Ren, X.-C.; Wang, P.; Yu, S.-H., Macroscopic multifunctional graphene-based hydrogels and aerogels by a metal ion induced self-assembly process. *ACS Nano* **2012,** *6*, (3), 2693-703.

98. Korhonen, J. T.; Kettunen, M.; Ras, R. H. A.; Ikkala, O., Hydrophobic nanocellulose aerogels as floating, sustainable, reusable, and recyclable oil absorbents. *ACS Applied Materials & Interfaces* **2011,** *3*, (6), 1813-6.

99. Basak, S.; Nandaa, J.; Banerjee, A., A new aromatic amino acid based organogel for oil spill recovery. *Journal of Materials Chemistry* **2012,** *22*, (23), 11658-11664.

100. Zhu, Q.; Pan, Q.; Liu, F., Facile removal and collection of oils from water surfaces through superhydrophobic and superoleophilic Sponges. *Journal of Physical Chemistry* **2011,** *115*, (35), 17464-17470.

101. Gui, X.; Cao, A.; Wei, J.; Li, H.; Jia, Y.; Li, Z.; Fan, L.; Wang, K.; Zhu, H.; Wu, D., Soft, highly conductive nanotube sponges and composites with controlled compressibility. *ACS Nano* **2010,** *4*, (4), 2320-2326.

102. Zhua, L.; Lia, C.; Wanga, J.; Zhangb, H.; Zhanga, J.; Shena, Y.; Lia, C.; Wanga, C.; Xieb, A., A simple method to synthesize modified Fe3O4 for the removal of organic pollutants on water surface. *Applied Surface Science* **2012,** *258*, (17), 6326-6330.

103. Zhu, Q.; Tao, F.; Pan, Q., Fast and selective removal of oils from water surface via highly hydrophobic core-shell Fe2O3@C nanoparticles under magnetic field. *ACS Applied Materials & Interfaces* **2010,** *2*, (11), 3141-6.

104. Klaine, S. J.; Koelmans, A. A.; Horne, N.; Carley, S.; Handy, R. D.; Kapustka, L.; Nowack, B.; Kammer, F. v. d., Paradigms to assess the environmental impact of

manufactured nanomaterials. *Environmental Toxicology and Chemistry* **2012,** *31*, (1), 3-14.

105. Bradford, S. A.; Simunek, J.; Bettahar, M.; Van Genuchten, M. T.; Yates, S. R., Modeling colloid attachment, straining, and exclusion in saturated porous media. *Environmental Science & Technology* **2003,** *37*, (10), 2242-50.

106. Gargiuloa, G.; Bradfordb, S.; Šimůnekc, J.; Ustohala, P.; Vereeckena, H.; Klumppa, E., Bacteria transport and deposition under unsaturated conditions: The role of the matrix grain size and the bacteria surface protein. *Journal of Contaminant Hydrology* **2007,** *92*, (3), 255-273.

107. Davis, K. A.; Charleux, B.; Matyjaszewski, K., Preparation of block copolymers of polystyrene and poly (t -butyl acrylate) of various molecular weights and architectures by atom transfer radical polymerization. *Journal of Polymer Science. Part A, Polymer chemistry* **2000,** *38*, (12), 2274-2283.

108. Sun, S.; Zeng, H.; Robinson, D. B.; Raoux, S.; Rice, P. M.; Wang, S. X.; Li, G., Monodisperse MFe2O4 (M = Fe, Co, Mn) nanoparticles. *Journal of the American Chemical Society* **2004,** *126*, (1), 273-9.

109. Bao, N.; Shen, L.; Wang, Y.; Padhan, P.; Gupta, A., A facile thermolysis route to monodisperse ferrite nanocrystals. *Journal of the American Chemical Society* **2007,** *129*, (41), 12374-5.